Mapping pan-Arctic landfast sea ice stability using Sentinel-1 interferometry

Dyre O. Dammann[1], Leif E.B. Eriksson[1], Andrew R. Mahoney[2], Hajo Eicken[3], Franz J. Meyer[2]

[1]Department of Space, Earth and Environment, Chalmers University of Technology, Gothenburg, 412 96, Sweden
[2]Geophysical institute, University of Alaska Fairbanks, Fairbanks, 99775, USA
[3]International Arctic Research Center, University of Alaska Fairbanks, Fairbanks, 99775, USA

Correspondence to: Dyre O. Dammann (dyre.dammann@chalmers.se)

Abstract. Arctic landfast sea ice has undergone substantial changes in recent decades, affecting ice stability, and including potential impacts on ice travel by coastal populations and on industry ice roads. We present a novel approach for evaluating landfast sea ice stability on a pan-Arctic scale using Synthetic Aperture Radar Interferometry (InSAR). Using Sentinel-1 images from spring 2017, we discriminate between bottomfast, stabilized, and non-stabilized landfast ice over the main marginal seas of the Arctic Ocean (Beaufort, Chukchi, East Siberian, Laptev, and Kara Seas). This approach draws on the evaluation of relative changes in interferometric fringe patterns. This first comprehensive assessment of Arctic bottomfast sea ice extent has revealed that most of the bottomfast sea ice is situated around river mouths and coastal shallows. The Laptev and East Siberian Seas dominate the aerial extent, covering roughly 4.1 and 5.1 thousand km^2, respectively. These seas also contain the largest extent of stabilized and non-stabilized landfast ice, but are subject to the largest uncertainties surrounding the mapping scheme. Even so, we demonstrate the potential for using InSAR for assessing the stability of landfast ice in several key regions around the Arctic, providing a new understanding of how stability may vary between regions. InSAR-derived stability may serve for strategic planning and tactical decision support for different uses of coastal ice. In a case study of the Nares Strait, we demonstrate that interferograms may reveal early-warning signals for the break-up of stationary sea ice.

1 Introduction

1.1 Landfast sea ice stability and stakeholder dependence

Sea ice is an important component of Arctic ecosystems and provides important functions as a climate regulator (Screen and Simmonds, 2010), habitat for marine biota (Thomas, 2017), and a platform for coastal populations (Krupnik et al., 2010). During the last century, an expansion of transportation and resource extraction have led to increased human presence in the Arctic and further diversification of ice use (Eicken et al., 2009). The recent retreat of sea ice observed over the past several decades (Stroeve et al., 2012; Comiso and Hall, 2014; Meier et al., 2014) has already resulted in widespread consequences for ice users (ACIA, 2004; Aporta and Higgs, 2005; Fienup-Riordan and Rearden, 2010; Orviku et al., 2011; Druckenmiller et al., 2013), as well as increasing hazards (Ford et al., 2008; Eicken and Mahoney, 2015). At the same time, the related increased accessibility to Arctic waters (Stephenson et al., 2011) is leading to more ship traffic and resource exploration (Lovecraft and Eicken, 2011; Eguíluz et al., 2016). It is further recognized that sea ice conditions for future Arctic marine operations will be challenging, and will require substantial monitoring and improved observations (Arctic Council, 2009). This improvement will require observations at a local and regional scale, in order to provide assessment of environmental hazards and effective emergency response (Eicken et al., 2011). Most of the Arctic Ocean is dominated by drifting pack ice, whereas stationary landfast ice occupies much of the Arctic coastlines between roughly November and June, depending on location (Figure 1; Yu et al., 2014). Sections of landfast ice, often from several

km to hundreds of km wide, are held in place by grounded ridges, islands, or coastline morphology, such as embayments or fjords. Similar to drifting pack ice, landfast ice has declined significantly during the last few decades, particularly in terms of delayed freeze-up in the Beaufort (Mahoney et al., 2014) and Laptev (Selyuzhenok et al., 2015) Seas, as well as significantly reduced extent in the Chukchi Sea (Mahoney et al., 2014). Later freeze-up critically impacts stakeholders through reduced stability of landfast ice

5   in response to fewer grounded ridges capable of withstanding wind, ocean, or ice forcing (Dammann, 2017). Previous research suggests that landfast ice stability can be expressed in terms of combined frictional resistance provided by relevant grounding or attachment points (e.g., islands and grounded ridges; Mahoney et al., 2007; Druckenmiller, 2011). Although landfast ice is stationary, it deforms at the cm- to m-scale, on timescales of days to months, due to forcing from wind, currents, and drifting ice (Dammann et al., 2016). Its stability in part determines the rate at which the ice deforms, and ultimately, the severity of break-out

10   events or magnitude of structural defects. We suggest that landfast sea ice can be further categorized into three regimes, defined through their respective stability: (1) bottomfast ice; (2) floating ice enclosed in lagoons or fjords, or sheltered by point features such as grounded ridges or islands; and (3) floating ice extensions (Table 1). A typical landfast ice regime is illustrated in Figure 2, where the stability of the landfast ice area decreases from the coast toward the open ocean (Dammann et al., 2016).

Bottomfast sea ice can grow laterally to the km-scale during winter, depending on local bathymetry (Solomon et al., 2008; Stevens et

15   al., 2010). This bottomfast ice allows for heat loss from the sea floor, and is therefore an integral part of aggregating and maintaining subsea permafrost (Solomon et al., 2008; Stevens et al., 2008; Stevens et al., 2010; Stevens, 2011), as well as controlling coastal stability/morphology (Are and Reimnitz, 2000; Eicken et al., 2005). Bottomfast ice is also relevant for fish, as it reduces habitable shallow waters during winter (Hirose et al., 2008), and for on-ice operations, as it can support a much larger load than floating ice. High to moderately stable landfast ice is of relevance to industrial (Potter et al., 1981) and subsistence ice use (Druckenmiller et

20   al., 2013), as well as for habitats (Tibbles et al., 2018). Ringed seals, for instance, are dependent on stable landfast ice for denning (Smith, 1980). Low-stability ice is potentially relevant for ocean-based operations, such as shipping through trans-Arctic passages close to the coast, where patches of landfast ice occasionally break off and drift into nearby shipping lanes, potentially causing hazards. Even areas hundreds of km from landfast ice can be impacted through the failure of ice arches.

Ice arches may be considered an additional zone of "temporarily stabilized pack ice." Ice arches form when ice moving through a

25   narrow passage experiences flow stoppage as a result of confining pressure and begins to behave like landfast ice, though potentially without cohesive strength between individual floes (Hibler et al., 2006). Ice arches typically form between November and March (Moore and McNeil, 2018), and can block the export of ice through straits as wide as 100 km (Melling, 2002). When formed, such arches represent a significant obstacle to marine traffic, due to the high confining pressures that make icebreaking impossible for all but the most powerful vessels. Arches can in some locations prevail into the following season (Melling, 2002),

30   but typically collapse in July–August (Kwok, 2005). Conversely, their break-up can lead to the advection of large amounts of thick multiyear ice into high-traffic shipping routes (Barber et al., 2018), creating a well-known hazard (Bailey, 1957; Wilson et al., 2004; Howell et al., 2013). Recent and ongoing sea ice decline is leading to an increasing presence of thinner ice in the Canadian Archipelago (Haas and Howell, 2015), and weaker ice due to warmer temperatures (Melling, 2002) may lead to earlier breaching of ice arches. This could result in a larger amount of advected ice with potentially longer travel paths, increasing the severity of

35   such events (Melling, 2002; Barber et al., 2018). One location of particular interest is the Nares Strait, situated between Greenland and Ellesmere Island, featuring a seasonal ice arch (Kwok, 2005; Kwok et al., 2010) with important implications for the multiyear ice budget of the Arctic Ocean (Kwok et al., 2010). This stability is also relevant for destinational cargo shipping in the Arctic, as less stable, thinner ice is easier to break through, resulting in opportunities for docking in areas of landfast ice. For navigating through landfast ice, stabilization through ridging is also important to identify, as ridges can be problematic to navigate and are

40   often associated with hazards (Hui et al., 2017).

1.2 Remote sensing of landfast ice stability

Satellite remote sensing is an important tool for measuring ice conditions in the Arctic, including the mapping of landfast ice (Muckenhuber and Sandven, 2017). Optical/thermal satellite data, such as from the Advanced Very High Resolution Radiometer (AVHRR), were used to produce operational ice charts until the early 1990s, when SAR was introduced into the charting production (Yu et al., 2014) as a superior data set, thanks to its independence from light and weather conditions and its higher (~100 m) resolution—both advantageous to stakeholders (Eicken et al., 2011). Different techniques exist to map the boundaries of landfast sea ice, typically derived by evaluating unchanged sections of ice between consecutive SAR backscatter scenes (Johannessen et al., 2006; Giles et al., 2008; Mahoney et al., 2014). In addition to its use in the mapping of landfast ice, SAR backscatter can also discriminate between multiyear and first-year ice (Onstott, 1992) and identify different roughness regimes (Dammann et al., 2017). SAR has also been used to estimate the advection of ice through straits in the Canadian Archipelago (Melling, 2002; Kwok, 2006; Howell et al., 2013). However, SAR backscatter typically does not give information pertaining to the stability of landfast ice or "temporarily stabilized pack ice" since the internal movement of the landfast ice is too small (mm/day) to be identified with change detection.

SAR interferometry (InSAR) is a signal processing technique, which extracts the phase difference between two SAR images acquired with similar viewing geometries. This phase difference (typically referred to as interferometric phase) can either signify topography if acquisitions are separated in space (i.e., non-zero perpendicular baseline), or measure the line-of-sight motion if acquisitions are separated in time (non-zero temporal baseline; Bamler and Hartl, 1998; Ferretti et al., 2007). InSAR has been successfully used to map landfast ice edges by identifying areas of slow motion (Meyer et al., 2011). InSAR has also provided information pertaining to landfast ice dynamics (Li et al., 1996; Morris et al., 1999; Vincent et al., 2004; Marbouti et al., 2017) and topography (Dammann et al., 2017;Dierking et al., 2017) by evaluating the phase change between acquisitions. InSAR has also been shown to reveal plausible rheologies for landfast ice (Dammert et al., 1998), and has been used to determine the origin of internal ice stresses (Berg et al., 2015). Combined with inverse modeling, InSAR enables us to determine ice deformation modes (Dammann et al., 2016), rates, and the associated stress and fracture potentials (Dammann et al., 2018b).

These studies have demonstrated (1) the potential of InSAR as a tool for assessing landfast ice dynamics and stability through local case studies and (2) its utility as a planning tool for on-ice operations (Dammann et al., 2018a; Dammann et al., 2018b). They have also laid the foundation for applying InSAR on a larger scale, potentially as a means for generating operational information products and evaluating long-term trends. The coverage and access to InSAR-compatible SAR scenes has been an obstacle in the past, but has improved significantly since the launch of Sentinel-1 (the suitability of Sentinel-1 for automatic SAR processing has been shown, e.g., in Meyer et al., 2015). In this study, we explore InSAR as a tool for providing pan-Arctic information on ice stability, which is relevant to subsea permafrost, biological habitats, and sea ice use. The goal of this work is to determine Sentinel-1 interferometric data availability along substantial parts of the circumpolar coastlines, and to explore their applicability for consistently mapping landfast sea ice stability zones in different geographic regions. We further explore limitations of the technology and possible applications.

2 Data and methods

2.1 InSAR principles

The interferometric phase may be related to lateral (e.g., thermal contraction or displacement due to compressional or shear forces) or vertical (e.g., through buckling or tidal displacement) sea ice motion that occurs in between the acquisition times for the two SAR images. A phase signature can sometimes also be attributed to factors not related to surface motion, such as atmospheric

phase delay. Of the phase change attributed to motion, only displacement in line-of-sight direction (Δr_{LOS}) results in a phase change $\Delta\Phi_{disp}$, according to $\Delta\Phi_{disp} = 4\pi\,\Delta r_{LOS}/\lambda$. The observed phase is measured within the wrapped interval of $[0; 2\pi]$. The interferogram is a series of fringes representing the projection of the true three-dimensional ice motion onto the line-of-sight vector. The orientation of fringes can be used to interpret the direction of the three-dimensional motion field, and fringe spacing is an indicator of the deformation rate. The interpretation of observed fringe patterns is, however, not straightforward, and it typically requires the use of an inverse model (Dammann et al., 2016). The interferometric phase values will only be useful if scattering elements remain largely unchanged throughout the time interval bracketed by the image pairs used in processing. InSAR phase stability, referred to as InSAR coherence, depends largely on topography coupled with perpendicular baseline, as well as the temporal stability of the scatterers on the ground surface. Coherence ranges between 0 (pure noise) and 1 (no noise), and serves as a measure of the quality of the interferogram. Coherence is generally high if scatterers remain unchanged, and low if there is significant change in the scattering medium (Meyer et al., 2011).

2.2 Sentinel-1 data

This study uses Sentinel-1, a constellation of two C-band SAR systems (Sentinel-1A and B) in operation since 2014 and 2016, respectively, with a repeat-pass interval of six to twelve days, depending on whether both or just one of the satellites acquire data. Thanks to a free-and-open data policy and large spatial coverage, we obtained Sentinel-1 acquisitions for five marginal seas of the Arctic Ocean, enabling mapping of landfast sea ice on a pan-Arctic scale. All images used were captured in interferometric wideswath (IW) mode, with a single-look resolution of roughly 3 m × 22 m in slant range and azimuth, respectively, and a ~250 km swath width. Images were acquired almost exclusively between March and May 2017 (see supplementary data for full list of images used). We acquired over one hundred SAR images, covering nearly the entire continental coastlines of the Beaufort, Chukchi, East Siberian, Laptev, and Kara Seas. To reduce computational costs, we omitted Greenland, some island groups, and the Canadian Archipelago, which are characterized by extensive coastline lengths. In this work, we focused on the Alaska and Russian marginal seas of the Arctic Ocean. These coastlines have high economic significance for the shipping and natural resource industries, and also feature dynamically diverse ice regimes. Large areas of bottomfast ice are expected in these regions. Except for one approximately 50 km-long section of coast in the Kara Sea and the eastern Laptev Sea, multiple InSAR compatible pairs were available for the specified time frame. This allowed us to select interferograms centered around the end of April, when most Arctic landfast ice is at its maximum extent and thickness.

In addition to images obtained for the large-scale mapping of stability zones, a series of six consecutive image pairs were acquired covering the Nares Strait and the break-up of an ice arch during spring 2017. This image sequence featured a six-day temporal baseline covering a timespan of thirty-six days.

2.3 Data processing

All the complex Sentinel-1 data was processed to obtain backscatter, in order to visually interpret features (e.g., landfast ice edge, fracturing, ice roughness and types). Data was further processed for interferometry. Depending on the perpendicular baseline, sea ice topography can have a modest impact on the phase difference. Due to tight baseline limits (<50 m standard deviation) for the Sentinel-1 constellation, and since sea ice topography rarely exceeds 10 m, impacts for interferogram interpretation are minimal for the data shown here. In this work we predominately employed acquisitions with a temporal lag of either twelve or twenty-four days, depending on data availability. For this timespan, the coherence over landfast ice was found to be generally high, due to its stationary nature. However, coherence loss was evident in some areas—in particular in the Chukchi Sea, such as in the Kotzebue Sound. This was likely predominantly due to surface melt, as air temperature reached above freezing between SAR acquisitions.

Other possible contributing reasons for coherence loss in this region could include ice motion, subsurface ice thinning from river runoff, and low signal-to-noise ratio. Significant decorrelation can also occur in late spring, as the onset of melt causes substantial changes in the scattering medium. In this work, we obtained images as close to late April as possible. This timeframe was found to be ideal for our purpose, as ice thickness is near its maximum, leading to maximum stability and minimizing impacts from the onset of melt. To ensure a realistic representation of an operationally-produced synoptic, contiguous pan-Arctic interferogram, we did not attempt to derive alternative interferograms (i.e., different time periods) in cases of low coherence.

All backscatter images and interferograms in this work were produced using a standard Sentinel-1 workflow in Gamma software (Werner et al., 2000). The IW images initially consist of independent bursts and swaths, which we combined to utilize full extent of the acquisition. We further coregistered pairs of acquisitions, to ensure images cover exactly the same area with sub-pixel accuracy. Images were then multi-looked, averaging 10 px in range and 2 px in azimuth, resulting in reduced speckle and a final pixel spacing of roughly 23×28 m. Next, spectral filtering was performed to ensure both images comprise the same spectral range, reducing phase noise in the final interferogram. The interferometric phase was calculated for each pixel of the coregistered and filtered images. Furthermore, the expected phase ramp in cross-track direction from a stationary flat earth surface was removed. The phase noise of the final interferogram was reduced using an adaptive phase filter (Goldstein and Werner, 1998). The result was fifty-two interferograms, covering almost the entire coastline between the Canadian Archipelago and the Barents Sea.

2.4 Mapping landfast ice stability zones

In this work, we evaluated relative ice stability based on fringe spacings within individual interferograms. This allowed us to identify variations within an area imaged under largely the same conditions (e.g., close to the same wind and ocean forcing). Trends from higher to lower fringe density will likely correspond to increasing ice stability. Therefore, interferograms can provide information related to the spatial variations in stability. Meyer et al. (2011) demonstrated that interferometry can be used to map the landfast ice based on a coherent phase response. Their work also suggested that fringe patterns are significantly impacted by grounded ridges and reduced fringe density. Dammann et al. (2018c) further showed that bottomfast ice can be mapped based on a near-zero phase change where ice is frozen to the seafloor. We built on this work by suggesting that InSAR can be used to map three different zones of relative stability: bottomfast ice, stabilized ice, and non-stabilized ice (Table 1). These three zones are subjectively and manually mapped without the use of specific threshold values.

Bottomfast ice is identified with near-zero phase change in the interferogram. It can often be distinguished from adjacent floating ice commonly featuring a non-zero phase change or low coherence (Figure 3a). The shoreward boundary of bottomfast ice is difficult to obtain from the interferogram alone, since the phase signatures over bottomfast ice and low-laying coastal areas are similar. The use of the landmask (Wessel and Smith, 1996) is not ideal, since subtle coastal features such as sediment bars are often not captured. We therefore delineated the coastline (i.e., shoreward boundary of bottomfast ice) using the backscatter signature in a composite image with backscatter and phase (Figure 3b). Plotting bottomfast ice with the landmask can thus give the wrongful appearance that (1) areas of near-zero phase should have been mapped as bottomfast and (2) bottomfast ice appears in sporadic areas along the coast separated by floating ice.

We could often identify stabilized ice by a stark fringe discontinuity between different fringe densities (Figure 3c). However, in some regions, changes in stability are more gradual between zones (Figure 6c and 7c). Mapping of such regions are therefore more subjective and possibly less exact. In cases lacking stark fringe discontinuities, stabilized ice is also mapped in regions featuring a very slight phase response with no clear fringe patterns (Figure 3d).

Non-stabilized ice is identified as landfast ice (i.e., areas featuring relatively high interferometric coherence) otherwise not marked as bottomfast or stabilized ice. Non-stabilized ice commonly features clear fringe patterns (Figure 3e).

2.5 Validation areas and data

The Beaufort Sea coast of Alaska was used for validation, as landfast sea ice in this area includes all three stability zones (bottomfast, stabilized, and non-stabilized), and ample validation data is available from previous studies. Alaska's Beaufort Sea coast is of major interest in the context of local and indigenous ice use, as well as industry resource exploration and extraction. Some areas along this coastline feature similar landfast ice extent over time scales from months to years. It was found that these regions ("nodes") of consistent landfast ice extent are often tied to the location of the 20-m isobath, a water depth associated with the grounding of pressure ridges stabilizing the landfast ice (Mahoney et al., 2014). Indigenous knowledge and a field study also indicate persistent grounded ridges in the location of the node closest to Utqiaġvik, Alaska (Meyer et al., 2011). We also evaluated our results near Stolbovoy Island in the Laptev Sea. This area features a shoal of <10-m water depth, leading to earlier formation of fast ice than the surrounding areas (Selyuzhenok et al., 2015), likely due to the formation of grounded ridges on the shoal and resulting in increased stability.

3 Results

3.1 Evaluating landfast ice stability zones

We constructed a series of Sentinel-1 interferograms along the coastlines of five marginal seas in the Arctic Ocean during 2017: the Beaufort, Chukchi, East Siberian, Laptev, and Kara Seas. As seen in the in the interferograms (Figures 4-8), landfast sea ice varies substantially between the seas in terms of the extent and interferometric fringe density.

The landfast sea ice extent in the Beaufort Sea ranges from almost zero up toward 100 km (Figure 4a). River outlets such as the Colville and Mackenzie Deltas feature extensive regions of bottomfast ice several kilometers wide (Figure 4b, c). Bottomfast ice is also prominent in many lagoons along the coast. Much of the floating ice along the coast from Prudhoe Bay to Point Barrow is stabilized. This stabilized ice can be identified by a stark fringe discontinuity separating regions of different fringe density and stability (Figure 4a, b). The line of discontinuity features several seaward points, an expected pattern surrounding grounded ridges. This is because grounded ridges result in a shoreward increase in stability that does not extend to areas immediately to the side of the ridges (the along-shore direction). Examples of likely grounding points are indicated with white arrows in Figure 4b, and similar patterns are also apparent near the Mackenzie Delta (Figure 4c). The landfast ice in the eastern part of the Beaufort Sea also consists of large areas of stabilized ice. Here, the landfast ice is noticeably sheltered by land features, resulting in lower density fringes (Figure 4d).

Landfast sea ice in the Chukchi Sea is generally less extensive than in the Beaufort Sea, particularly along the Russian coast (Figure 5a). Bottomfast ice in the Chukchi is constrained mostly to lagoons. Some of these lagoons, such as the Kasegaluk, consist almost exclusively of bottomfast ice (Figure 5b). Only a few areas of landfast ice appear to be stabilized, including the northern coast of Alaska near Peard Bay (Figure 5c), and the southern Chukchi Sea near Shishmaref (Figure 5d). The Chukchi Sea consists predominantly of non-stabilized ice, with the most extensive region of landfast ice situated off shore from the village of Shishmaref (Figure 5d). The Chukchi Sea features coherence loss in several regions such as the Kotzebue Sound (Figure 5a).

The landfast ice in the East Siberian Sea is more extensive than in the Chukchi and Beaufort Seas and can extend over 100 km from shore (Figure 6a). Bottomfast ice is also more extensive than in the Beaufort and Chukchi Seas. The bottomfast ice in the East Siberian Sea follows several sections of coastline even tens of km away from major rivers, though most of the bottomfast ice is situated near the Kolyma and Indigirka Deltas (Figure 6b). In contrast to the Beaufort and Chukchi Seas, stabilized ice extends several tens of km offshore without being sheltered by coastline morphology or islands (Figure 6c). These large areas also lack clear indications of the presence of grounded ridges (Figure 6d).

Landfast ice in the Laptev Sea, similar to the East Siberian Sea, extends upwards of 100 km from shore (Figure 7a). Here, most of the bottomfast ice is situated around river outlets and in particular near the Lena Delta, extending tens of km from shore (Figure 7b). This delta features a large amount of small, low-lying land areas (e.g., gravel islands) only partly covered by the landmask. This has made it problematic to delineate all areas of bottomfast ice, and led to more approximate delineations than in the other

5   deltas mapped. On the east side of the Lena Delta and south of the Great Lyakhovsky Island, there are extensive sections of stabilized ice (Figure 7c). Some regions of the eastern Laptev Sea lack a clear discontinuity, but at the same time feature locally reduced fringe density, indicative of stabilized ice (Figure 7c). We also considered these areas to be stabilized (Figure 7c), though possibly as a result of different ice type or thickness, rather than through grounding or sheltering. However, one offshore area is clearly identified as stable by a lack of consistent fringe patterns and a clear discontinuity, likely due to grounded ridges (Figure

10 7d).

Landfast ice in the Kara Sea features much smaller ice extent than the other Russian Seas (Figure 8a). Bottomfast ice is also much less prevalent and largely situated near the Pyasina River (Figure 8b). The landfast ice extends tens of km from shore, predominately in areas supported by offshore islands and archipelagos (Figure 8c and d). In these archipelagos, the ice confined by islands is largely stabilized (Figure 8c).

15 Interferograms have enabled the mapping of landfast ice stability zones based on subjective interpretation of interferometric fringes (Figure 9). The resulting stability map allows for a large-scale comparison and analysis of bottomfast, stabilized, and non-stabilized landfast ice, within and between the different seas. For this comparison, we have calculated the area of each stability zone (Table 2). However, it is important to note these area calculations are not complete, as the analysis omitted some island groups and included some data gaps.

20 Most areas with extensive bottomfast ice reaching several km from shore are located either in the vicinity of river deltas or within lagoons. The East Siberian Sea and its three large river systems (the Indigirka, Bogdashkina, and Kolyma Rivers) contain the most bottomfast ice of the regions considered here. The Laptev Sea also contains a large area of bottomfast sea ice. Together, the Laptev and East Siberian Seas contain over half (~57 %) of the total areal extent of bottomfast ice calculated, while the Chukchi Sea features the lowest extent of bottomfast ice of the regions considered here. Bottomfast ice is predominately situated in lagoons.

25 Stabilized ice was found in all marginal seas (Figure 9), though its relative contributions to overall landfast ice extent varied widely. The largest extent of stabilized landfast ice in our study region was found in the Laptev and East Siberian Seas. These regions feature particularly large continuous areas of stabilized ice labeled A-F in Figure 9. Even so, as we delineated here, the Beaufort Sea is the only sea that features more stabilized ice than non-stabilized ice. This is likely attributed to the large grounded sections, as well as areas sheltered by coastal morphology. The Laptev Sea also features large areas confined by coastlines. However, in the

30 Laptev sea, these regions also commonly feature non-stabilized ice. Meanwhile a large part of the landfast ice in the Kara Sea is mapped as stabilized, largely due to the fraction of landfast ice situated between islands and archipelagos. With a relatively narrow landfast ice extent as compared to other seas and absence of regions of sheltered ice, the Chukchi Sea contains the lowest total extent of stabilized ice.

In the Chukchi Sea, we identified the vast majority of landfast ice as non-stabilized (Figure 9), resulting in our largest areal fraction

35 (non-stabilized ice / stabilized ice). Though the largest total areas of non-stabilized ice can be found in the Laptev and East Siberian Seas. Here, the distinction between stabilized and non-stabilized landfast ice is not as straightforward as in the Beaufort and Chukchi Seas, due to a lack of clear boundaries between areas of different fringe densities. Even so, it is clear that landfast ice extent in the East Siberian and Laptev Seas is dominated by vast areas of non-stabilized ice. However, unlike the Chukchi Sea, we also identified significant areas of stabilized landfast ice along these two seas. The Kara Sea features predominately non-stabilized

40 ice along the coast and along the outer margins of archipelagos.

3.2 Evaluating stability of temporarily stabilized pack ice

Sentinel-1 SAR backscatter imagery captured the location and break-up of the ice arch in Nares Strait in 2017 (Figure 12). This break-up event occurred relatively early as compared with past events (Kwok, 2005), partly in response to thinner ice conditions and northerly winds (Moore and McNeil, 2018). The arch appeared stable on 6 May (Figure 12b), before eventually failing sometime before 12 May (Figure 12c) as seen in the SAR backscatter images. The interferograms revealed the ice deformation around the location of fracture up until the failure event. As seen in the interferograms, the ice arch features various levels of cm- to m-scale deformation and fractures prior to break-up, resulting in fringe discontinuities (Figure 13a) most pronounced near the arch terminus to the south. Near the failure line, there was no sign of a fringe discontinuity up until 12 April (Figure 13a), when the interferogram displays near cross-track parallel fringes, indicating compression towards the terminus (Figure 13b). There is a significant contrast in fringe density on either side of the line, which may be indicative of a fracture, where the ice to the west is being compressed more rapidly than the ice close to the coast. The interferogram between 18 and 24 April features widespread coherence loss, possibly due to continued compression (Figure 13c). Deformation is less severe from 24 April on, when fringe density is significantly reduced. However, we did notice a fringe discontinuity to the east of the failure line, featuring perpendicular intermediate fringe patterns following to late April (see arrows in Figure 13d). These patterns develop further into circular patterns often associated with vertical lifts and depressions (Figure 13e), before the whole arch appears to fail through shear motion along this same fault (Figure 13f).

4 Discussion

4.1 Validating stability zones with areas of known ice stability

The InSAR technique to map bottomfast sea ice was thoroughly validated in several regions by Dammann et al. (2018c). The high stability of these regions can be inferred from the ice resting on the sea floor. However, other stability zones (i.e., stabilized and non-stabilized ice) are based on relative stability, in terms of whether the ice is anchored or sheltered. Determining absolute stability (i.e., whether an area is stable enough for a specific use, such as ice roads) would be problematic using fringe density alone. This is because there are many factors that affect fringe density in addition to stability, including changing wind and ocean currents, satellite viewing geometry, and the prevalent mode of ice deformation (Dammann et al., 2016). A measure of whether ice is practically stable would also depend on specific stakeholders and their dependence on stability. For example, on shorter time scales, industry ice roads would be able to accommodate less strain than community ice trails, due to different modes of transportation and user-specific needs. Further steps to identify such thresholds are outlined in Dammann et al. (2018a).

There is limited information that can be used to validate these stability classes—namely, the separation between stabilized- and non-stabilized ice. Even so, we compared our mapping approach here with one region in the Beaufort and one in the Laptev Sea with areas of known stabilization points. We examined a backscatter mosaic from three images (8, 15, and 17 Apr) along the Beaufort Sea coast. These images exhibit, in certain locations, a sharp discontinuity in backscatter, which can identify the location of the landfast ice edge (see white arrows in Figure 10a).

The landfast ice edge identified using backscatter is consistent with the three "nodes" (A-C) identified by Mahoney et al. (2007a; 2014; our Figure 10b). These nodes signify a persistent landfast ice edge, believed to be a result of reoccurring grounded ice features (Mahoney et al., 2014). The ice shoreward of these three nodes is expected as stabilized, because grounded ridges are known to stabilize landfast ice, leading to reduced strain shoreward of the grounding points (Mahoney et al., 2007; Druckenmiller, 2011). Interferograms exhibit a phase response, suggesting stabilized ice directly shoreward of node A and C (Figure 10c). Here, node A is known to correspond to the location of large grounded ridges, offering stability to the ice cover (Meyer et al., 2011).

Nodes B and C are also expected to be regions of persistent grounded ridges since the nodes coincide roughly with the 20-m isobath (Mahoney et al., 2014). However, ice directly shoreward of node B appears non-stabilized, with stabilization only further in. This may be due to the reduced keel depth of ridges in 2017, or possibly reduced grounding strength of ridges present in B. Certain sections of the border between stabilized and non-stabilized ice extend relatively far from the coast (see black arrows in Figure 10d). At these points, the stability is higher than adjacent areas with the same distance from shore. This is consistent with increased stability behind grounded ridges.

Although the landfast ice edge can in some instances be mapped using a single backscatter image, stabilized ice cannot easily be discriminated from non-stabilized ice. This is apparent when comparing grounding locations as obtained with InSAR with backscatter images (see black arrows in Figure 10a). It is also worth noting that relying on backscatter to discriminate landfast or drifting ice only works in some cases. There must be noticeable differences in backscatter between landfast and drifting ice, or a severely deformed landfast ice edge as a result of shear interaction with the pack ice (Druckenmiller et al., 2013).

Similar patterns indicating grounded ridges were found in the Laptev Sea, where an April interferogram shows a section of stabilized ice roughly 100 km offshore (see "A" in Figure 11). The full area extent of the stabilized ice cannot be determined due to limited data availability in the region, and one interferogram had to be acquired as early as February, before this region had stabilized. Stabilized ice is expected in this region, which features a large shoal, earlier ice formation than surrounding areas, and grounded ridges (Selyuzhenok et al., 2015). The location of this large shoal, along with smaller ones, are obtained from Jakobsson et al. (2012) and displayed in Figure 11b. Here, it is apparent that even some of the smaller shoals are associated with stabilized ice (see "B" and "C" in Figure 11b). It is also clear that the extensive stabilized ice that stretches out halfway between Great Lakhovsky Island and Stolbovoy Island is potentially anchored between the coast and the shallow areas (see "D" in Figure 11b).

4.2 Methodological limitations for mapping stability zones

There are a number of sources of uncertainty that affect our map of landfast ice and its relative stability. Dammann et al. (2018c) have determined that in some instances, bottomfast ice has to be approximated on the sub-km-scale due to ambiguities associated with low fringe density or fringes parallel to the bottomfast ice edge. We also acknowledge that small islands or sandbars not represented by our landmask may be erroneously identified as bottomfast ice. We have reduced such errors by not mapping areas that appears to be low-laying land in the SAR backscatter images. However, discriminating between ice and low-laying land can be difficult based on strictly SAR. Here, other remote sensing systems such as optical could be applied to further reduce biases from coastline errors. In areas where the landmask does not appear to fit the coastline due to errors or coastline changes, mapping intricate coastal morphology can be a time-consuming task—hence mapping on a pan-Arctic scale will inevitably contain inaccuracies. It is also worth mentioning that the other stability zones are mapped against the landmask, also likely resulting in errors. However, as the extent of these zones are larger, the relative contribution of such errors will be much smaller.

In this work, we did not apply strict mapping thresholds to distinguish between stabilized and non-stabilized ice, but rather made subjective determinations based on fringe patterns. This approach works well in the Chukchi and Beaufort Seas, where regions of low fringe density lie adjacent to the coast or bottomfast ice and can be easily distinguished from regions of higher fringe density. However, in some regions, especially in the Russian Arctic, there is often a lack of distinct boundaries between regions of different fringe spacing, introducing ambiguities between stabilized and non-stabilized ice on scales from km to even tens of km (Figures 6c and 7c). The difficulty distinguishing in these two zones may result from reduced pack ice interaction along the Russian shelf, given the predominately divergent ice regimes (Reimnitz et al., 1994; Alexandrov et al., 2000; Jones et al., 2016). This generally results in reduced ice forcing and landfast ice strain in contrast to the western Arctic. Such ice regime is expected to feature reduced dynamically-induced strain (and therefore fewer interferometric fringes) in non-stabilized ice, making it appear more stable. This

is visible in the different fringe densities of the non-stabilized ice in Figures 4d and 6d). Additionally, the greater extent of landfast ice on the shoreward side of the grounding points provides a greater fetch, which may cause stabilized ice on the Russian Shelf to exhibit higher fringe densities than in the Chukchi or Beaufort Seas. This suggests that there is likely a spectrum of landfast ice stability. Additional zones may be necessary to fully characterize landfast ice regimes in different regions for different ice uses or

5   research aims. Expanding on the classes presented here would likely require a different set of evaluation criteria for fringes, depending on regions. Additional data such as bathymetry would also likely strengthen such analysis.

We have focused on some examples with possibly suboptimal classification. One potential candidate for reclassification is landfast ice in sheltered bays, such as the Khatanga Gulf in the western Laptev Sea, which exhibited predominantly high fringe densities (Figure 7a). Hence, the Khatanga Gulf was identified largely as non-stabilized, despite being nearly landlocked (Figure 9). Due to

10   the shallow water in this region, it is likely that the high fringe density is caused in part by vertical motion associated with tides and coastal set up. Since vertical motion has less impact on stability in well-confined landfast ice, such examples suggest the potential need for an additional zone of stability, allowing higher fringe densities in coastally confined regions. Such additional classification would depend on other datasets such as a landmask or bathymetry to identify the level of restricted ice movement in response to likely forcing conditions. Another, larger-scale example is the eastern Laptev sea, which is an area of landfast ice

15   sheltered by the New Siberian Islands and is typically considered stable (Eicken et al., 2005). However, based on relatively high fringe density, particularly offshore of the Lena Delta, we classified much of the landfast ice in this region as non-stabilized (Figure 9). This suggests the criteria for stabilized ice used in this analysis is different than in Eicken et al. (2005), and can provide new information related to stability in the region. Based on the overall fringe counts and patterns, the majority of the phase response is due to lateral displacement and potentially only partially due to vertical displacement (circular fringe patterns with low density—

20   see Dammann et al., 2016) due to tidal motion. It is possible that landfast ice in this region may be less stable than previously thought, and that a "partially stabilized" zone may be appropriate. This would be consistent with a recent SAR backscatter analysis of landfast ice in the Laptev Sea (Selyuzhenok et al., 2017), which showed that areas identified as landfast ice in operational ice charts may actually contain pockets of partly mobile ice. This was shown for the month after initial landfast ice formation, but could possibly result in more dynamic ice throughout spring due to reduced ice thickness.

25   Sensitivity to specific atmospheric and oceanographic conditions during the time period between SAR acquisitions may place a limitation on the number of stability zones that can be mapped. For example, in the absence of dynamic interaction with pack ice, there may be little difference in fringe spacing between landfast ice seaward and shoreward of stabilizing anchor points. Without evaluating the phase response for each area of interest in detail during different forcing scenarios, it may be difficult to understand under what conditions the ice remains stable. Classification of stability based on relative differences in fringe density is also

30   complicated by the use of non-simultaneous interferograms to provide complete coverage of a region. The interferograms used here were obtained as close to maximum ice extent and stability as possible (roughly late April), but sometimes had to be obtained as early as February. Fringe density tends to decrease over the winter as the ice thickens (Dammann et al., 2016). Hence, the use of interferograms based on different dates can aid interpretation by confirming consistent fringe patterns and discontinuities that identify temporal changes. Temporal changes result in phase discontinuities at the image stitchings not related to different stability

35   zones, which further complicates the mapping process.

Sentinel-1 IW imagery is predominantly acquired over land, so it is likely not possible to construct interferograms away from the coast, for extensive landfast ice approaching the 250 km IW swath, such as that in the East Siberian Sea. Data availability further restricts the temporal baseline between images to a minimum of twelve days, though this now represents a shorter period than past work identifying landfast ice (Mahoney et al., 2004; Meyer et al., 2011; Dammann et al., 2016). Further studies should investigate

40   the effect of different temporal baselines on the stability product. A shorter baseline will result in higher temporal resolution.

However, with a shorter baseline (e.g., Sentinel-1 6-day baseline), mapping of the seaward landfast ice edge may incorporate stationary pack ice. A longer baseline will result in lower interferometric coherence. With a twelve-day baseline, some regions, such as the Kotzebue Sound region, already feature consistent coherence loss. Such regions can most often be identified through a spatially inconsistent progression, from high to a complete loss of coherence. In such cases, the mapping of landfast ice type boundaries is not possible. It is worth mentioning this technique can only be used before the onset of melt, when widespread coherence loss occurs. Therefore, it is not possible to evaluate the retreat of bottomfast ice or the reduction of ice stability in response to melt.

5 Conclusion

In a time of rapidly changing sea ice conditions and continued interest in the Arctic from a range of stakeholders, we stress the need for new assessment strategies to enable safe and efficient use of sea ice. InSAR is gaining growing attention in the sea ice scientific community, and here we demonstrate its value for identifying zones of landfast ice stability. We are also highlighting the application of InSAR for the development of operational sea ice information products, for both long-term strategic planning and short-term tactical decisions. Using interferograms generated by a standardized workflow, we show that three stability zones of landfast ice can be identified based on fringe density and continuity, indicative of differential ice motion occurring between SAR acquisitions. Along the Beaufort Sea coast of Alaska, we find that the landfast ice regime can be well described with three stability zones: bottomfast ice, where the sea ice is frozen to or resting on the seabed; stabilized ice, which is floating but sheltered by coastlines or anchored by islands or grounded ridges; and non-stabilized ice, which represent floating extensions seaward of any anchoring points. These findings are supported by comparison with the location of stable "nodes," identified through analysis of hundreds of landfast ice edge positions over the period 1996-2008. Not only does this provide some validation of our results, but it demonstrates the ability of InSAR to capture useful information in just two snapshots, compared to previously requiring analysis over many years.

Based on our findings, it is likely that InSAR-derived maps could provide substantial value as a stand-alone product for some regions such as the Beaufort Sea. With that said, the stability zones in the Beaufort Sea and the Russian Arctic appear to be qualitatively different. This makes it challenging to directly adapt the proposed scheme to the East Siberian and Laptev Seas, which are associated with substantial uncertainties. Even so, we demonstrate the data availability and application of this InSAR-based approach, which can provide added value to ice charts and other products. In ice charting, multiple information products are evaluated with local knowledge to create final products. Similarly, the value of InSAR may be greatly enhanced by linking with other products (e.g., InSAR time series analysis, SAR-based and optical remote sensing products, local knowledge, coastal morphology and bathymetry, and atmospheric and ocean forcing data).

The use of a standardized workflow facilitates large-scale application of this approach, which we demonstrate on a near-pan Arctic scale using fifty-two Sentinel-1 acquisition pairs during spring 2017. This has allowed us to map the same zones of landfast ice in the Beaufort, Chukchi, East Siberian, Laptev, and Kara Seas. To our knowledge, our results represent the first mapping of bottomfast ice extent at this scale and the first attempt at any scale to map the extents of different landfast ice stability zones. It also enabled us to estimate and compare the total area covered by each stability zone in each marginal sea. However, we note that these comparisons are based on the assumptions that the landfast ice regimes in all these seas can be well described by the same three stability zones. Although the delineation of different zones can be subjective, in particular in the Russian Arctic, our results clearly show that not all landfast ice is equally stable. Here, InSAR is potentially able to detect small-scale motions up to hundreds of km from shore that have previously been overlooked. In addition, there are uncertainties associated with the exact mapping of

stability zones—in particular in terms of the exact delineation between stabilized and non-stabilized ice in the East Siberian and Laptev Seas. Here, the boundaries between stabilized and non-stabilized ice are more difficult to discriminate, likely due to fewer pinning points where the ice is grounded or supported. Therefore, what we present here is not an operational ice chart, but the ability and application to discriminate stability classes on a pan-Arctic scale using InSAR.

5   The method presented in this work has a broad set of potential applications for monitoring, including subsea permafrost, biological habitats both beneath and above the ice surface, and ice use by a range of stakeholders. Bottomfast ice is important because it helps for aggregating subsea permafrost, which serves to constrain the location of permafrost-rich shorelines. Utilizing InSAR, it is likely possible to monitor changes in bottomfast ice over time, with significant implications for erosion and spring flooding and the release of methane hydrates. We argue the utility of InSAR and its potential applications also extend to maritime activities and

10   shipping. In regards to the latter, vessel traffic typically does not traverse landfast ice. However, the assessment of landfast ice stability and spatio-temporal extent can potentially aid the management of conflicting ice uses such as in the case of the access route to the Voisey's Bay mine in the Canadian Arctic, which cuts through the landfast ice that is part of a traditional Nunatsiavummiut use area (Bell et al., 2014).

With respect to ice users, sea ice navigation near or through landfast sea ice is presently predominately supported by sea ice charts

15   used to map areas occupied by landfast ice. However, these charts do not provide information about the relative stability of the ice. The information provided here would likely be useful in the context of navigation and support of on-ice operations. The InSAR-based approach described here can potentially provide support by identifying the following stability-related features:

1) Low-stability ice that may break off and drift into shipping lanes.

2) Grounded ridges that may be problematic for ice navigation, but at the same time may provide added stability for on-ice

20   operations.

3) Stable areas to use for equipment staging by coastal community hunters and industry.

4) Bottomfast ice for development of ice roads for transportation of heavy loads.

We further demonstrate the scientific and operational value of InSAR over sea ice through the examination of interferograms of ice arches. In this context, they can be considered part of an additional stability zone of quasi-landfast ice (i.e., "temporarily

25   stabilized pack ice"). Preliminary analysis of the Nares Strait ice arch in 2017 suggests that interferograms may reveal precursors to the failure of ice arches. We further speculate that InSAR tools can be developed to inform stakeholders of changing landfast ice stability and ice movement. Such applications would have potential value for an early warning system designed to alert ice users of hazards related to ice movement and break-out events. The use of inverse modeling may further help derive the small-scale strain field from interferograms, which may improve our ability to predict their failure. We expect that InSAR can provide

30   valuable information for stakeholders, enabling tracking of ice dynamics and stability on seasonal timescales. The ability to provide stability information to stakeholders also opens up for development of operational guidelines in terms of what stability zones should be prioritized or avoided.

This work builds on previous applications of InSAR to study landfast ice and demonstrates what can be achieved over large areas with a standardized workflow. 2017 was the first year Sentinel-1 covered the Arctic coast with the IW images necessary for this

35   analysis. If this coverage continues, there will be considerable opportunity for development beyond what is presented here, including development of automated methods for mapping and classifying landfast ice suitable for incorporation into operational ice charts. Furthermore, through additional analysis of landfast ice and ice arches subject to different forcing conditions, we anticipate improving our understanding of stabilizing and destabilizing mechanisms. This would allow the improved prediction of formation and break-up. Not only will this enhance the operational sea ice information available to stakeholders, but it also allows

40   us to better understand the response of coastal sea ice to a changing Arctic environment.

Acknowledgements

This work was funded by the Swedish National Space Agency (Dnr. 192/15). Sentinel-1 data are provided free of charge by the European Union Copernicus program and were downloaded through Alaska Satellite Facility (ASF). We thank Bill Hauer (ASF) for valuable data support and Christopher Stevens (SRK Consulting) and Joost van der Sanden (Canada Centre for Mapping and Earth Observation) for valuable guidance. We thank Nate Bauer and two anonymous reviewers who substantially contributed to improving this manuscript.

Competing interests

The authors declare that they have no conflict of interest.

References

ACIA: Impacts of a Warming Arctic, Arctic Climate Impact Assessment, Cambridge University Press, Cambridge, UK, 144 pp., 2004.

Alexandrov, V. Y., Martin, T., Kolatschek, J., Eicken, H., Kreyscher, M., and Makshtas, A. P.: Sea ice circulation in the Laptev Sea and ice export to the Arctic Ocean: Results from satellite remote sensing and numerical modeling, Journal of Geophysical Research: Oceans, 105, 17143-17159, 2000.

Aporta, C., and Higgs, E.: Satellite culture - Global positioning systems, inuit wayfinding, and the need for a new account of technology, Curr Anthropol, 46, 729-753, 10.1086/432651, 2005.

Arctic Council: Arctic marine shipping assessment, Protection of the Arctic Marine Environment Working Group (PAME), Akureyri, Island, 190, 2009.

Are, F., and Reimnitz, E.: An overview of the Lena River Delta setting: geology, tectonics, geomorphology, and hydrology, Journal of Coastal Research, 16, 1083-1093, 2000.

Bailey, W.: Oceanographic features of the Canadian Archipelago, Journal of the Fisheries Board of Canada, 14, 731-769, 1957.

Bamler, R., and Hartl, P.: Synthetic aperture radar interferometry, Inverse problems, 14, R1, 1998.

Barber, D., Babb, D., Ehn, J., Chan, W., Matthes, L., Dalman, L., Campbell, Y., Harasyn, M., Firoozy, N., and Theriault, N.: Increasing mobility of high Arctic sea ice increases marine hazards off the east coast of Newfoundland, Geophys Res Lett, 45, 2370-2379, 10.1002/2017GL076587, 2018.

Bell, T., Briggs, R., Bachmayer, R., and Li, S.: Augmenting Inuit knowledge for safe sea-ice travel—The SmartICE information system, 2014 Oceans'14 St. John's, Newfoundland, 2014, 1-9, 2014.

Berg, A., Dammert, P., and Eriksson, L. E. B.: X-Band Interferometric SAR Observations of Baltic Fast Ice, IEEE Transactions on Geoscience and Remote Sensing, 53, 1248-1256, 10.1109/TGRS.2014.2336752, 2015.

Comiso, J. C., and Hall, D. K.: Climate trends in the Arctic as observed from space, Wiley Interdisciplinary Reviews: Climate Change, 5, 389-409, 10.1002/wcc.277, 2014.

Dammann, D. O., Eicken, H., Meyer, F., and Mahoney, A.: Assessing small-scale deformation and stability of landfast sea ice on seasonal timescales through L-band SAR interferometry and inverse modeling, Remote Sens Environ, 187, 492-504, 10.1016/j.rse.2016.10.032, 2016.

Dammann, D. O.: Arctic sea ice trafficability - new strategies for a changing icescape, Ph.D. thesis, Department of Geosciences, University of Alaska Fairbanks, Fairbanks, Alaska, USA, 217 pp., 2017.

Dammann, D. O., Eicken, H., Saiet, E., Mahoney, A., Meyer, F., and George, J. C.: Traversing sea ice - linking surface roughness and ice trafficability through SAR polarimetry and interferometry IEEE Journal of Selected Topics in Applied Earth Observations and Remote Sensing, 11, 416-433, 10.1109/JSTARS.2017.2764961, 2017.

Dammann, D. O., Eicken, H., Mahoney, A., Meyer, F., and Betcher, S.: Assessing sea ice trafficability in a changing Arctic, Arctic, 71, 59-75, 10.14430/arctic4701, 2018a.

Dammann, D. O., Eicken, H., Mahoney, A., Meyer, F., Freymueller, J., and Kaufman, A. M.: Evaluating landfast sea ice stress and fracture in support of operations on sea ice using SAR interferometry, Cold Reg Sci Technol, 10.1016/j.coldregions.2018.02.001, 2018b.

Dammann, D. O., Eriksson, L. E. B., Mahoney, A., Stevens, C. W., Van der Sanden, J., Eicken, H., Meyer, F., and Tweedie, C.: Mapping Arctic bottomfast sea ice using SAR interferometry, Remote Sensing, 10(5), 720, 10.3390/rs10050720, 2018c.

Dammert, P. B. G., Lepparanta, M., and Askne, J.: SAR interferometry over Baltic Sea ice, Int J Remote Sens, 19, 3019-3037, 10.1080/014311698214163, 1998.

Dierking, W., Lang, O., and Busche, T.: Sea ice local surface topography from single-pass satellite InSAR measurements: a feasibility study, The Cryosphere, 11, 1967, 10.5194/tc-11-1967-2017, 2017.

Druckenmiller, M. L.: Alaska shorefast ice: interfacing geophysics with local sea ice knowledge and use, Ph.D. thesis, University of Alaska Fairbanks, Fairbanks, Alaska, 210 pp., 2011.

Druckenmiller, M. L., Eicken, H., George, J. C., and Brower, L.: Trails to the whale: reflections of change and choice on an Iñupiat icescape at Barrow, Alaska, Polar Geography, 36, 5-29, 10.1080/1088937X.2012.724459, 2013.

Eguíluz, V. M., Fernández-Gracia, J., Irigoien, X., and Duarte, C. M.: A quantitative assessment of Arctic shipping in 2010–2014, Scientific reports, 6, 30682, 2016.

Eicken, H., Dmitrenko, I., Tyshko, K., Darovskikh, A., Dierking, W., Blahak, U., Groves, J., and Kassens, H.: Zonation of the Laptev Sea landfast ice cover and its importance in a frozen estuary, Global and planetary change, 48, 55-83, 10.1016/j.gloplacha.2004.12.005, 2005.

Eicken, H., Lovecraft, A. L., and Druckenmiller, M. L.: Sea-Ice System Services: A Framework to Help Identify and Meet Information Needs Relevant for Arctic Observing Networks, Arctic, 62, 119-136, 10.14430/arctic126, 2009.

Eicken, H., Jones, J., Meyer, F., Mahoney, A., Druckenmiller, M. L., Rohith, M., and Kambhamettu, C.: Environmental security in Arctic ice-covered seas: from strategy to tactics of hazard identification and emergency response, Mar Technol Soc J, 45, 37-48, doi.org/10.4031/MTSJ.45.3.1, 2011.

Eicken, H., and Mahoney, A. R.: Sea Ice: Hazards, Risks, and Implications for Disasters, in: Coastal and Marine Hazards, Risks, and Disasters, edited by: Ellis, J. T., Sherman, D. J., and Shroder, J. F., Elsevier Inc., Amsterdam, Netherlands, 381-399, 2015.

Ferretti, A., Monti-Guarnieri, A., Prati, C., Rocca, F., and Massonet, D.: InSAR Principles-Guidelines for SAR Interferometry Processing and Interpretation, ESA Publications, TM-19, 2007.

Fienup-Riordan, A., and Rearden, A.: The ice is always changing: Yup'ik understandings of sea ice, past and present, in: SIKU: knowing Our Ice: Documenting Inuit Sea Ice knowledge and Use, edited by: Krupnik, I., Aporta, C., Gearheard, S., Laidler, G., and Holm, L. K., Springer, New York, 295-320, 2010.

Ford, J. D., Pearce, T., Gilligan, J., Smit, B., and Oakes, J.: Climate change and hazards associated with ice use in northern Canada, Arctic, Antarctic, and Alpine Research, 40, 647-659, 10.1657/1523-0430(07-040)[FORD]2.0.CO;2, 2008.

Giles, A. B., Massom, R. A., and Lytle, V. I.: Fast-ice distribution in East Antarctica during 1997 and 1999 determined using RADARSAT data, Journal of Geophysical Research: Oceans, 113, 10.1029/2007JC004139, 2008.

Goldstein, R. M., and Werner, C. L.: Radar interferogram filtering for geophysical applications, Geophys Res Lett, 25, 4035-4038, 10.1029/1998GL900033, 1998.

Haas, C., and Howell, S. E.: Ice thickness in the Northwest Passage, Geophys Res Lett, 42, 7673-7680, 10.1002/2015GL065704 2015.

5   Hibler, W., Hutchings, J., and Ip, C.: Sea-ice arching and multiple flow states of Arctic pack ice, Annals of Glaciology, 44, 339-344, 10.3189/172756406781811448, 2006.

Hirose, T., Kapfer, M., Bennett, J., Cott, P., Manson, G., and Solomon, S.: Bottomfast Ice Mapping and the Measurement of Ice Thickness on Tundra Lakes Using C-Band Synthetic Aperture Radar Remote Sensing, JAWRA Journal of the American Water Resources Association, 44, 285-292, 10.1111/j.1752-1688.2007.00161.x 2008.

10   Howell, S. E., Wohlleben, T., Dabboor, M., Derksen, C., Komarov, A., and Pizzolato, L.: Recent changes in the exchange of sea ice between the Arctic Ocean and the Canadian Arctic Archipelago, Journal of Geophysical Research: Oceans, 118, 3595-3607, 10.1002/jgrc.20265 2013.

Hui, F., Zhao, T., Li, X., Shokr, M., Heil, P., Zhao, J., Zhang, L., and Cheng, X.: Satellite-Based Sea Ice Navigation for Prydz Bay, East Antarctica, Remote Sensing, 9, 518, 10.3390/rs9060518, 2017.

15   Jakobsson, M., Mayer, L., Coakley, B., Dowdeswell, J. A., Forbes, S., Fridman, B., Hodnesdal, H., Noormets, R., Pedersen, R., and Rebesco, M.: The international bathymetric chart of the Arctic Ocean (IBCAO) version 3.0, Geophys Res Lett, 39, 10.1029/2012GL052219, 2012.

Johannessen, O. M., Alexandrov, V., Frolov, I. Y., Sandven, S., Pettersson, L. H., Bobylev, L. P., Kloster, K., Smirnov, V. G., Mironov, Y. U., and Babich, N. G.: Remote sensing of sea ice in the Northern Sea Route: studies and applications, Springer Science

20   & Business Media, Chichester, United Kingdom, 2006.

Jones, J. M., Eicken, H., Mahoney, A. R., Rohith, M. V., Kambhamettu, C., Fukamachi, Y., Ohshima, K. I., and George, J. C.: Landfast sea ice breakouts: Stabilizing ice features, oceanic and atmospheric forcing at Barrow, Alaska, Continental Shelf Research, 126, 10.1016/j.csr.2016.07.015, 2016.

Krupnik, I., Aporta, C., Gearheard, S., Laidler, G. J., and Holm, L. K.: SIKU: knowing our ice, Springer, New York, 2010.

25   Kwok, R.: Variability of Nares Strait ice flux, Geophys Res Lett, 32, 10.1029/2005GL024768 2005.

Kwok, R.: Exchange of sea ice between the Arctic Ocean and the Canadian Arctic Archipelago, Geophys Res Lett, 33, 10.1029/2006GL027094 2006.

Kwok, R., Toudal Pedersen, L., Gudmandsen, P., and Pang, S.: Large sea ice outflow into the Nares Strait in 2007, Geophys Res Lett, 37, L03502, 10.1029/2009GL041872, 2010.

30   Li, S., Shapiro, L., McNutt, L., and Feffers, A.: Application of Satellite Radar Interferometry to the Detection of Sea Ice Deformation, Journal of the Remote Sensing Society of Japan, 16, 67-77, 10.11440/rssj1981.16.153, 1996.

Lovecraft, A. L., and Eicken, H.: North by 2020: perspectives on Alaska's changing social-ecological systems, University of Alaska Press, Fairbanks, Alaska, 2011.

Mahoney, A., Eicken, H., Graves, A., Shapiro, L., and Cotter, P.: Landfast sea ice extent and variability in the Alaskan Arctic

35   derived from SAR imagery, Proceedings of the International Geoscience and Remote Sensing Symposium, Anchorage, AK, 2004, 2146-2149, 2004.

Mahoney, A., Eicken, H., and Shapiro, L.: How fast is landfast sea ice? A study of the attachment and detachment of nearshore ice at Barrow, Alaska, Cold Reg Sci Technol, 47, 233-255, 10.1016/J.Coldregions.2006.09.005, 2007.

Mahoney, A., Eicken, H., Gaylord, A. G., and Gens, R.: Landfast sea ice extent in the Chukchi and Beaufort Seas: The annual

40   cycle and decadal variability, Cold Reg Sci Technol, 103, 41-56, 10.1016/J.Coldregions.2014.03.003, 2014.

Marbouti, M., Praks, J., Antropov, O., Rinne, E., and Leppäranta, M.: A Study of Landfast Ice with Sentinel-1 Repeat-Pass Interferometry over the Baltic Sea, Remote Sensing, 9, 833, 10.3390/rs9080833, 2017.

Meier, W. N., Hovelsrud, G. K., Oort, B. E., Key, J. R., Kovacs, K. M., Michel, C., Haas, C., Granskog, M. A., Gerland, S., and Perovich, D. K.: Arctic sea ice in transformation: A review of recent observed changes and impacts on biology and human activity, Reviews of Geophysics, 52, 185-217, 10.1002/2013RG000431, 2014.

Melling, H.: Sea ice of the northern Canadian Arctic Archipelago, Journal of Geophysical Research: Oceans, 107, 10.1029/2001JC001102 2002.

Meyer, F. J., Mahoney, A. R., Eicken, H., Denny, C. L., Druckenmiller, H. C., and Hendricks, S.: Mapping arctic landfast ice extent using L-band synthetic aperture radar interferometry, Remote Sens Environ, 115, 3029-3043, 10.1016/J.Rse.2011.06.006, 2011.

Meyer, F. J., McAlpin, D., Gong, W., Ajadi, O., Arko, S., Webley, P., and Dehn, J.: Integrating SAR and derived products into operational volcano monitoring and decision support systems, ISPRS Journal of Photogrammetry and Remote Sensing, 100, 106-117, 10.1016/j.isprsjprs.2014.05.009, 2015.

Moore, G., and McNeil, K.: The early collapse of the 2017 Lincoln Sea ice arch inresponse to anomalous sea ice and wind forcing, Geophys Res Lett, 10.1029/2018GL078428, 2018.

Morris, K., Li, S., and Jeffries, M.: Meso-and microscale sea-ice motion in the East Siberian Sea as determined from ERS-I SAR data, Journal of Glaciology, 45, 370-383, 10.3189/S0022143000001878, 1999.

Muckenhuber, S., and Sandven, S.: Open-source sea ice drift algorithm for Sentinel-1 SAR imagery using a combination of feature tracking and pattern matching, The Cryosphere, 11, 1835, 10.5194/tc-11-1835-2017, 2017.

Onstott, R. G.: SAR and scatterometer signatures of sea ice, Microwave remote sensing of sea ice, 73-104, 1992.

Orviku, K., Jaagus, J., and Tõnisson, H.: Sea ice shaping the shores, Journal of Coastal Research, 681, 2011.

Potter, R., Walden, J., and Haspel, R.: Design and construction of sea ice roads in the Alaskan Beaufort Sea, Offshore Technology Conference, Houston, Texas, 1981

Reimnitz, E., Dethleff, D., and Nürnberg, D.: Contrasts in Arctic shelf sea-ice regimes and some implications: Beaufort Sea versus Laptev Sea, Marine Geology, 119, 215-225, 10.1016/0025-3227(94)90182-1, 1994.

Screen, J. A., and Simmonds, I.: The central role of diminishing sea ice in recent Arctic temperature amplification, Nature, 464, 1334-1337, 10.1038/nature09051, 2010.

Selyuzhenok, V., Krumpen, T., Mahoney, A., Janout, M., and Gerdes, R.: Seasonal and interannual variability of fast ice extent in the southeastern Laptev Sea between 1999 and 2013, Journal of Geophysical Research: Oceans, 120, 7791-7806, 10.1002/2015JC011135, 2015.

Selyuzhenok, V., Mahoney, A., Krumpen, T., Castellani, G., and Gerdes, R.: Mechanisms of fast-ice development in the south-eastern Laptev Sea: a case study for winter of 2007/08 and 2009/10, Polar Research, 36, 1411140, 10.1080/17518369.2017.1411140, 2017.

Smith, T. G.: Polar bear predation of ringed and bearded seals in the land-fast sea ice habitat, Canadian Journal of Zoology, 58, 2201-2209, 10.1139/z80-302, 1980.

Solomon, S. M., Taylor, A. E., and Stevens, C. W.: Nearshore ground temperatures, seasonal ice bonding, and permafrost formation within the bottom-fast ice zone, Mackenzie Delta, NWT, Proceedings of the Ninth International Conference on Permafrost, University of Alaska Fairbanks, Fairbanks, Alaska, 2008, 1675-1680, 2008.

Stephenson, S. R., Smith, L. C., and Agnew, J. A.: Divergent long-term trajectories of human access to the Arctic, Nat Clim Change, 1, 156-160, 10.1038/Nclimate1120, 2011.

Stevens, C. W., Moorman, B. J., and Solomon, S. M.: Detection of frozen and unfrozen interfaces with ground penetrating radar in the nearshore zone of the Mackenzie Delta, Canada, Proceedings of the Ninth International Conference on Permafrost, University of Alaska Fairbanks, Fairbanks, Alaska, 2008, 1711-1716, 2008.

Stevens, C. W., Moorman, B. J., and Solomon, S. M.: Interannual changes in seasonal ground freezing and near-surface heat flow beneath bottom-fast ice in the near-shore zone, Mackenzie Delta, NWT, Canada, Permafrost and Periglacial Processes, 21, 256-270, 10.1002/ppp.682 2010.

Stevens, C. W.: Controls on Seasonal Ground Freezing and Permafrost in the Near-shore Zone of the Mackenzie Delta, NWT, Canada, University of Calgary, 2011.

Stroeve, J. C., Serreze, M. C., Holland, M. M., Kay, J. E., Malanik, J., and Barrett, A. P.: The Arctic's rapidly shrinking sea ice cover: a research synthesis, Climatic Change, 110, 1005-1027, 10.1007/S10584-011-0101-1, 2012.

Thomas, D. N.: Sea ice, John Wiley & Sons, Chichester, United Kingdom, 2017.

Tibbles, M., Falke, J. A., Mahoney, A. R., Robards, M. D., and Seitz, A. C.: An In SAR habitat suitability model to identify overwinter conditions for coregonine whitefishes in Arctic lagoons, Transactions of the American Fisheries Society, 147(6), 1167-1178, doi.org/10.1002/tafs.10111, 2018.

Vincent, F., Raucoules, D., Degroeve, T., Edwards, G., and Abolfazl Mostafavi, M.: Detection of river/sea ice deformation using satellite interferometry: limits and potential, Int J Remote Sens, 25, 3555-3571, 10.1080/01431160410001688303, 2004.

Werner, C., Wegmüller, U., Strozzi, T., and Wiesmann, A.: Gamma SAR and interferometric processing software, Proceedings of the ERS-ENVISAT symposium, Gothenburg, Sweden, 2000, 1620

Wessel, P., and Smith, W. H.: A global, self-consistent, hierarchical, high-resolution shoreline database, Journal of Geophysical Research: Solid Earth, 101, 8741-8743, 10.1029/96JB00104, 1996.

Wilson, K. J., Falkingham, J., Melling, H., and De Abreu, R.: Shipping in the Canadian Arctic: other possible climate change scenarios, Proceedings of the International Geoscience and Remote Sensing Symposium, Anchorage, AK, 2004, 1853-1856, 2004.

Yu, Y., Stern, H., Fowler, C., Fetterer, F., and Maslanik, J.: Interannual Variability of Arctic Landfast Ice between 1976 and 2007, J Climate, 27, 227-243, 10.1175/JCLI-D-13-00178.1, 2014.
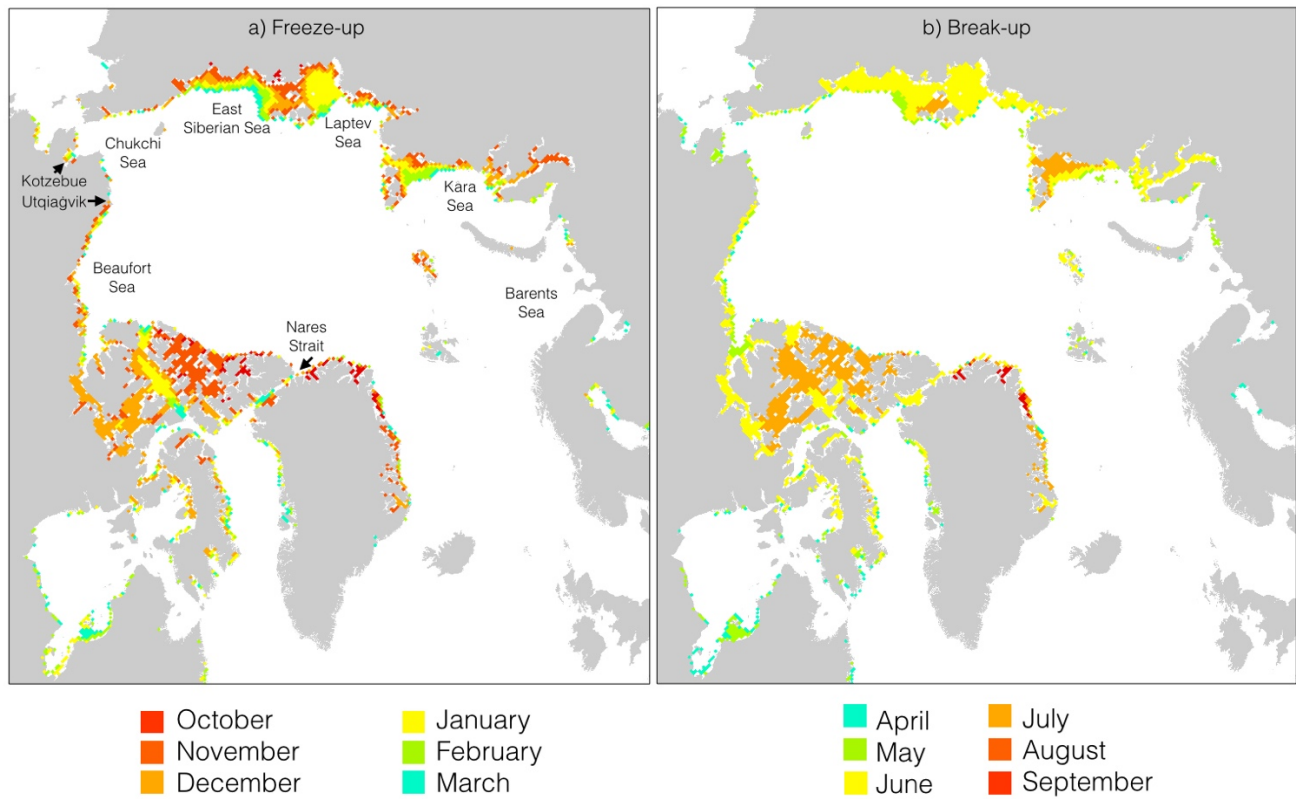
Figure 1: (a) Oct-Mar (Freeze-up) and (b) Apr-Sep (break-up) monthly mean landfast sea ice extent (1976-2007), derived from sea ice charts based on optical instruments and SAR. The data for this figure was obtained from the National Snow and Ice Data Center (Yu et al., 2014).
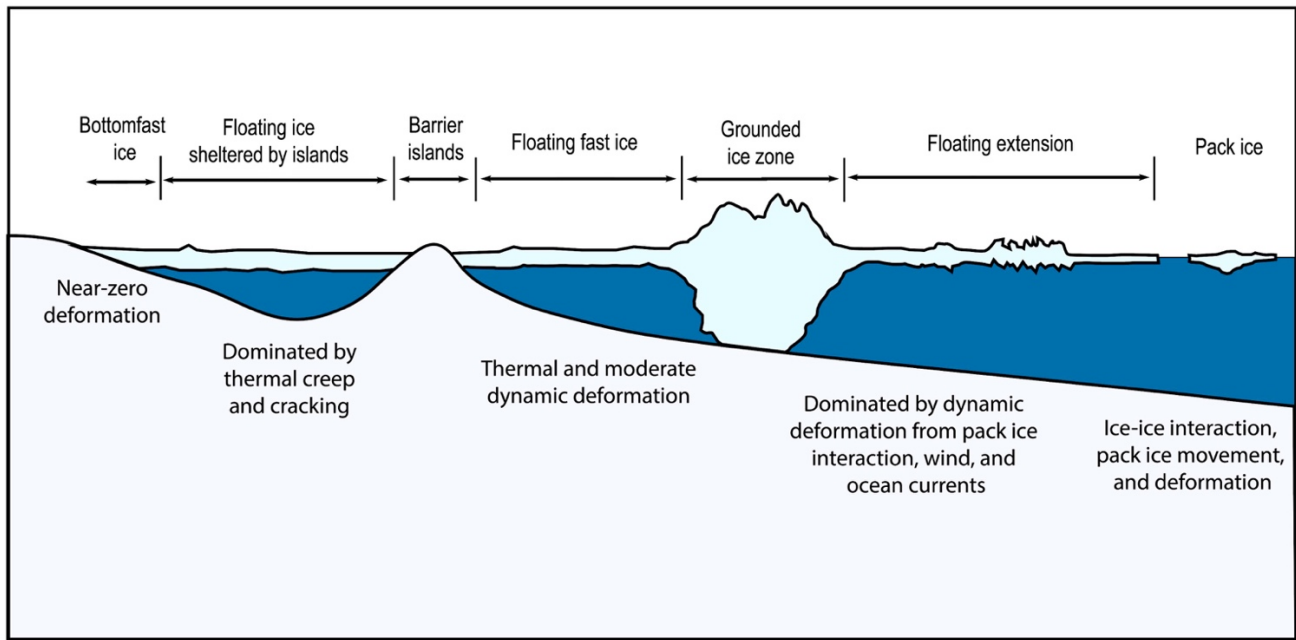
Figure 2: Conceptual scheme of landfast sea ice, where different regimes possess different levels of stability.
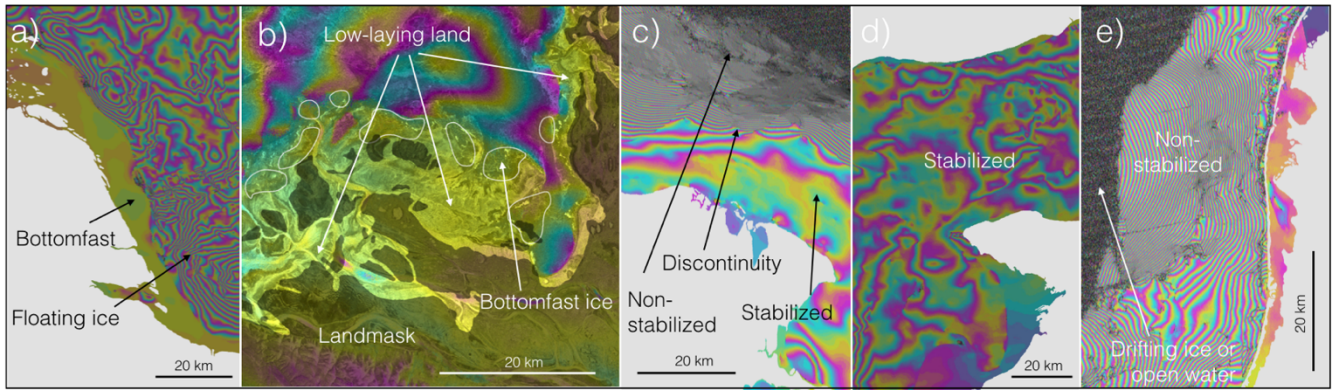
Figure 3: (a) Example of interferometric phase response over bottomfast ice. (b) Phase/backscatter composite near a delta. This example exhibits a poor match between the landmask (transparent black shading) and low-laying coastal areas. Here, bottomfast ice (white outline) had to be mapped against the coastline, as identified in the backscatter data. (c) Example of stabilized ice as identified based on a phase discontinuity. (d) Example of stabilized ice as identified by low fringe density and non-consistent fringe patterns. (e) Example of non-stabilized ice as identified by high fringe density. Land is masked out in light gray in a, c, d, and e.
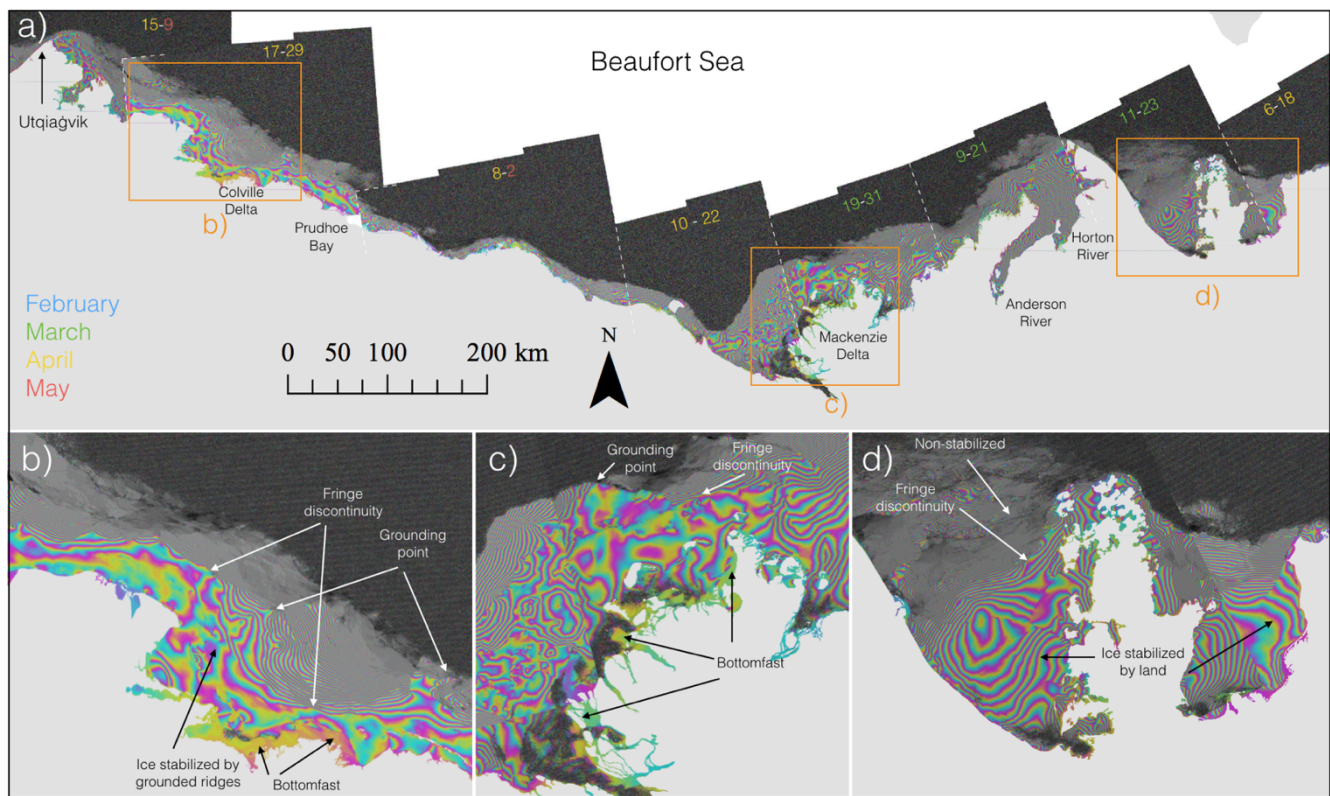
Figure 4: (a) Sentinel-1 interferograms derived from image pairs acquired over the Beaufort Sea between March and May, 2017. Numbers on images represent date ranges where the colors blue, green, yellow, and red signify the months of February-May, respectively. (b)-(d) Three enlarged areas identified in (a), further discussed in the text.
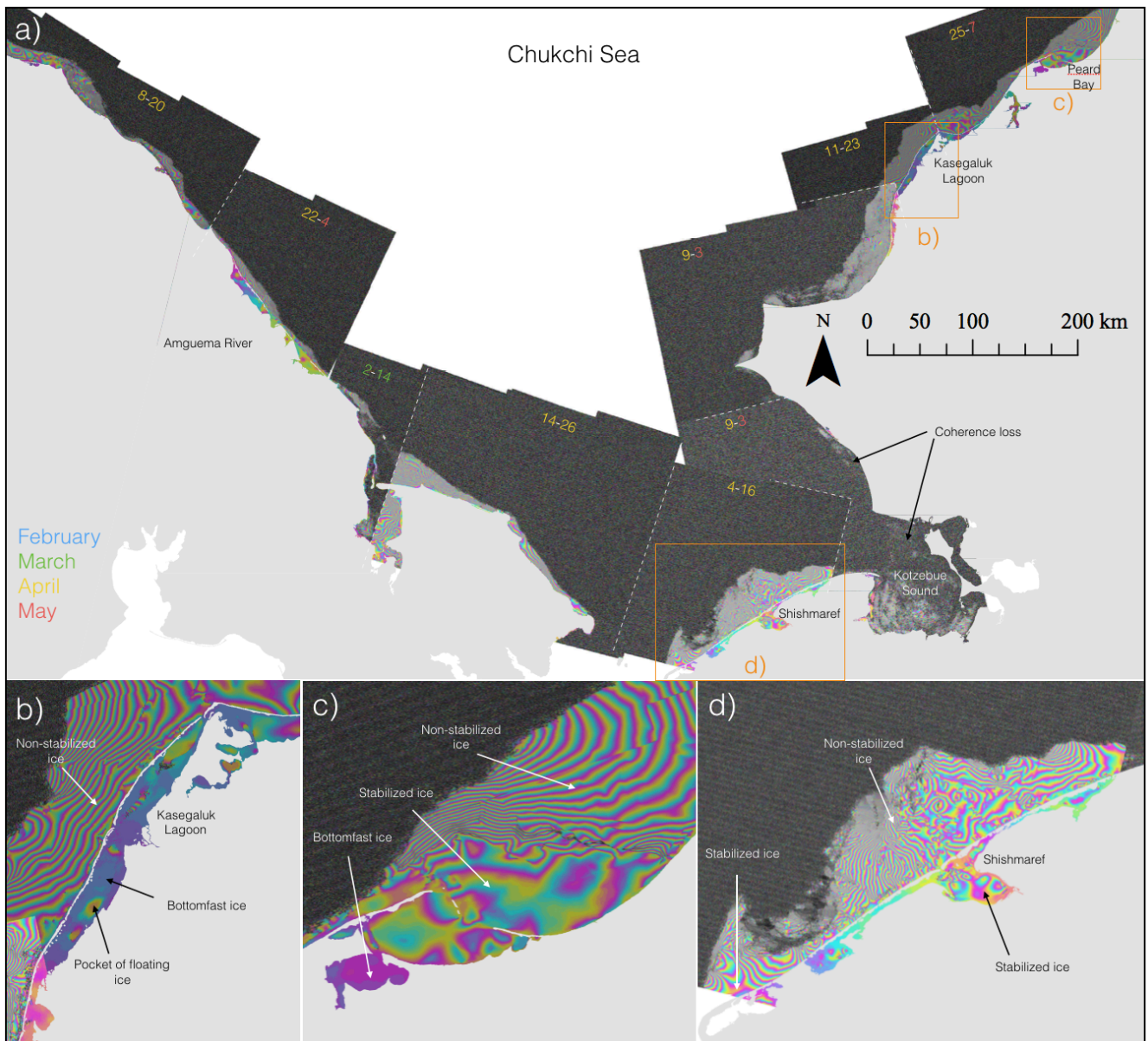
Figure 5: (a) Sentinel-1 interferograms derived from image pairs acquired over the Chukchi Sea between March and May, 2017. Numbers on images represent date ranges where the colors blue, green, yellow, and red signify the months of February-May, respectively. (b)-(d) Three enlarged areas identified in (a), further discussed in the text.
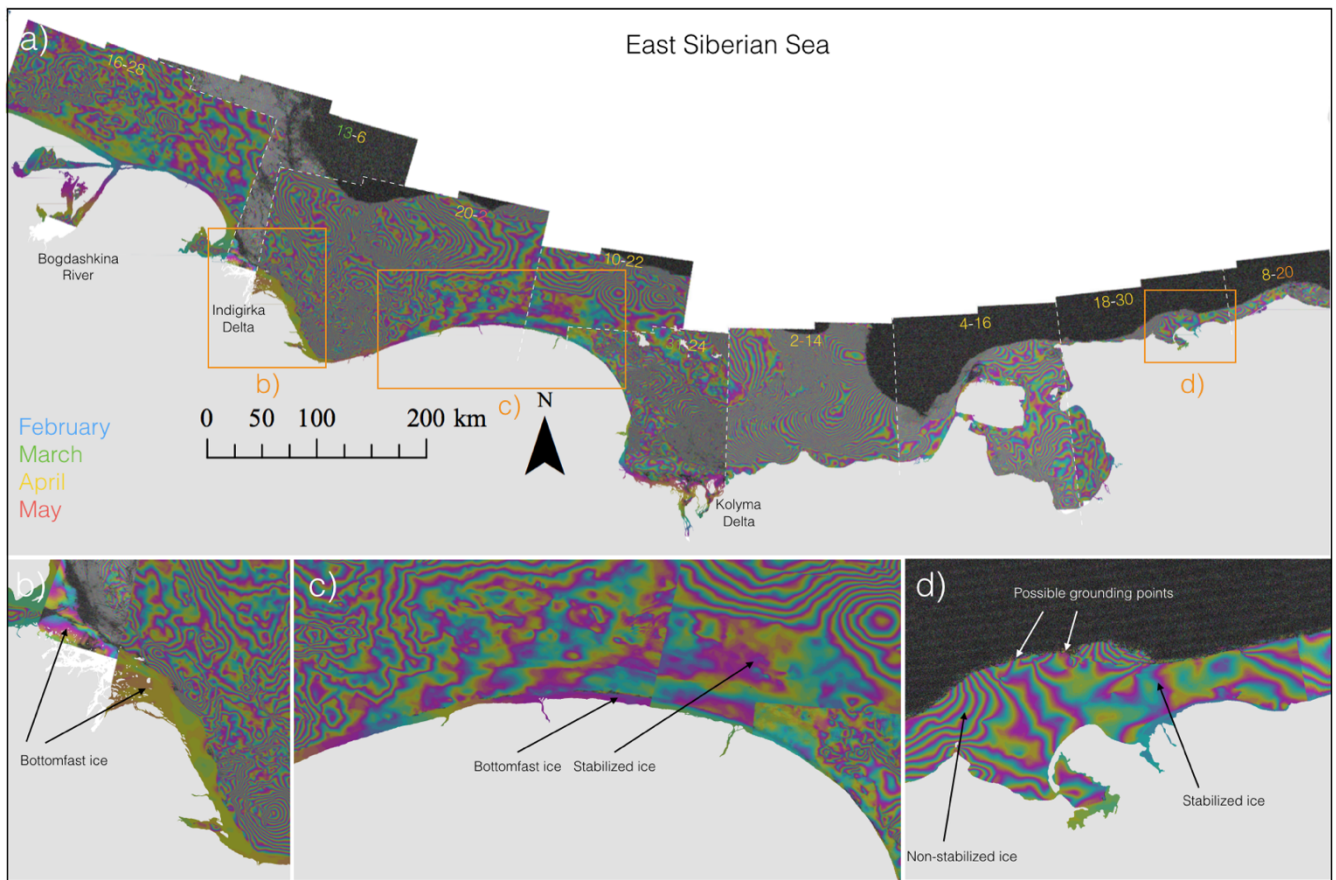
Figure 6: (a) Sentinel-1 interferograms derived from image pairs acquired over the East Siberian Sea between March and May, 2017. Numbers on images represent date ranges where the colors blue, green, yellow, and red signify the months of February-May, respectively. (b)-(d) Three enlarged areas identified in (a), further discussed in the text.
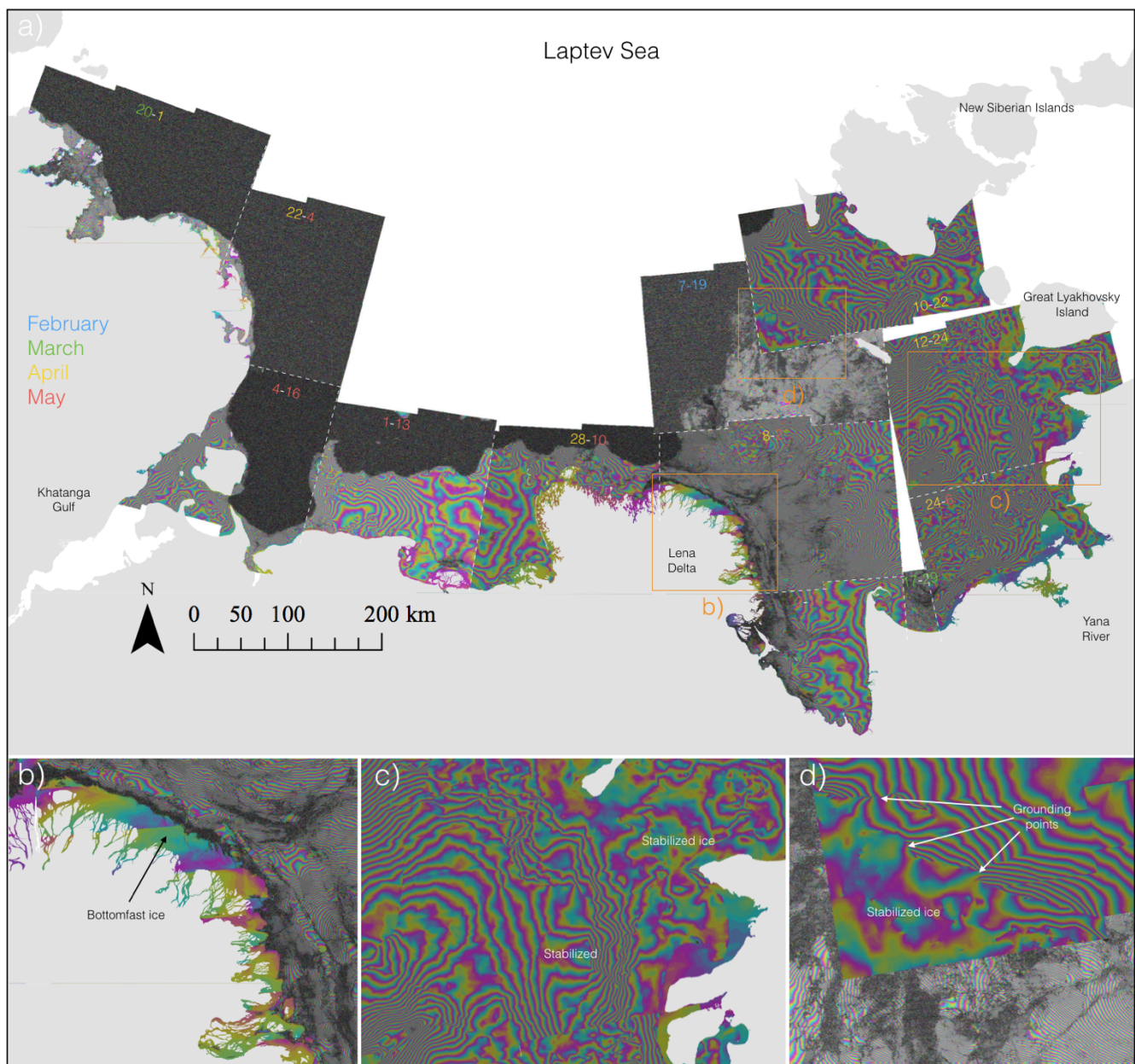
Figure 7: (a) Sentinel-1 interferograms derived from image pairs acquired over the Laptev Sea between February and May, 2017. Numbers on images represent date ranges where the colors blue, green, yellow, and red signify the months of February-May, respectively. (b)-(d) Three enlarged areas identified in (a), further discussed in the text.
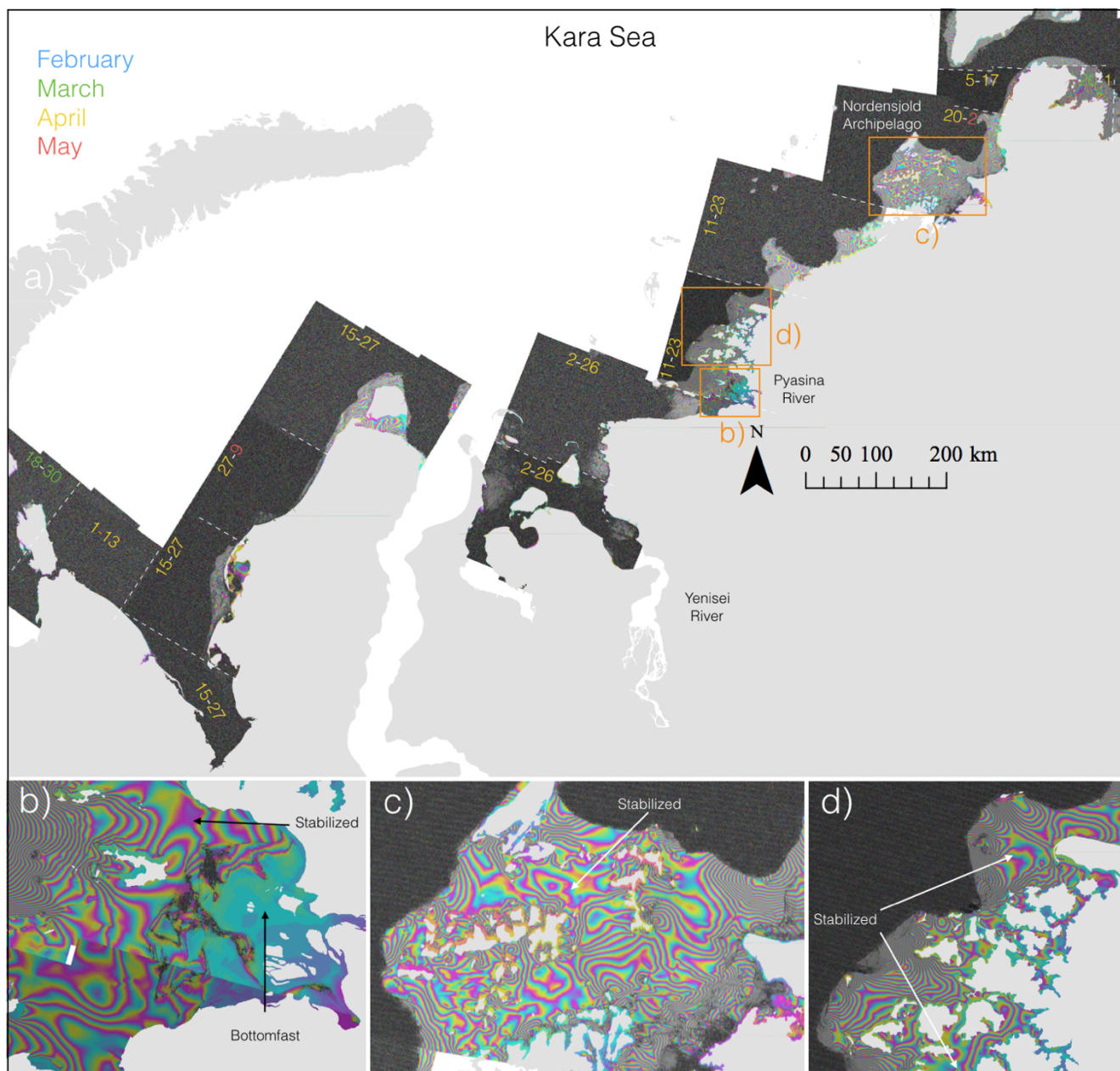
Figure 8: (a) Sentinel-1 interferograms derived from image pairs acquired over the Kara Sea between March and May, 2017. Numbers on images represent date ranges where the colors blue, green, yellow, and red signify the months of February-May, respectively. (b)-(d) Three enlarged areas identified in (a), further discussed in the text.
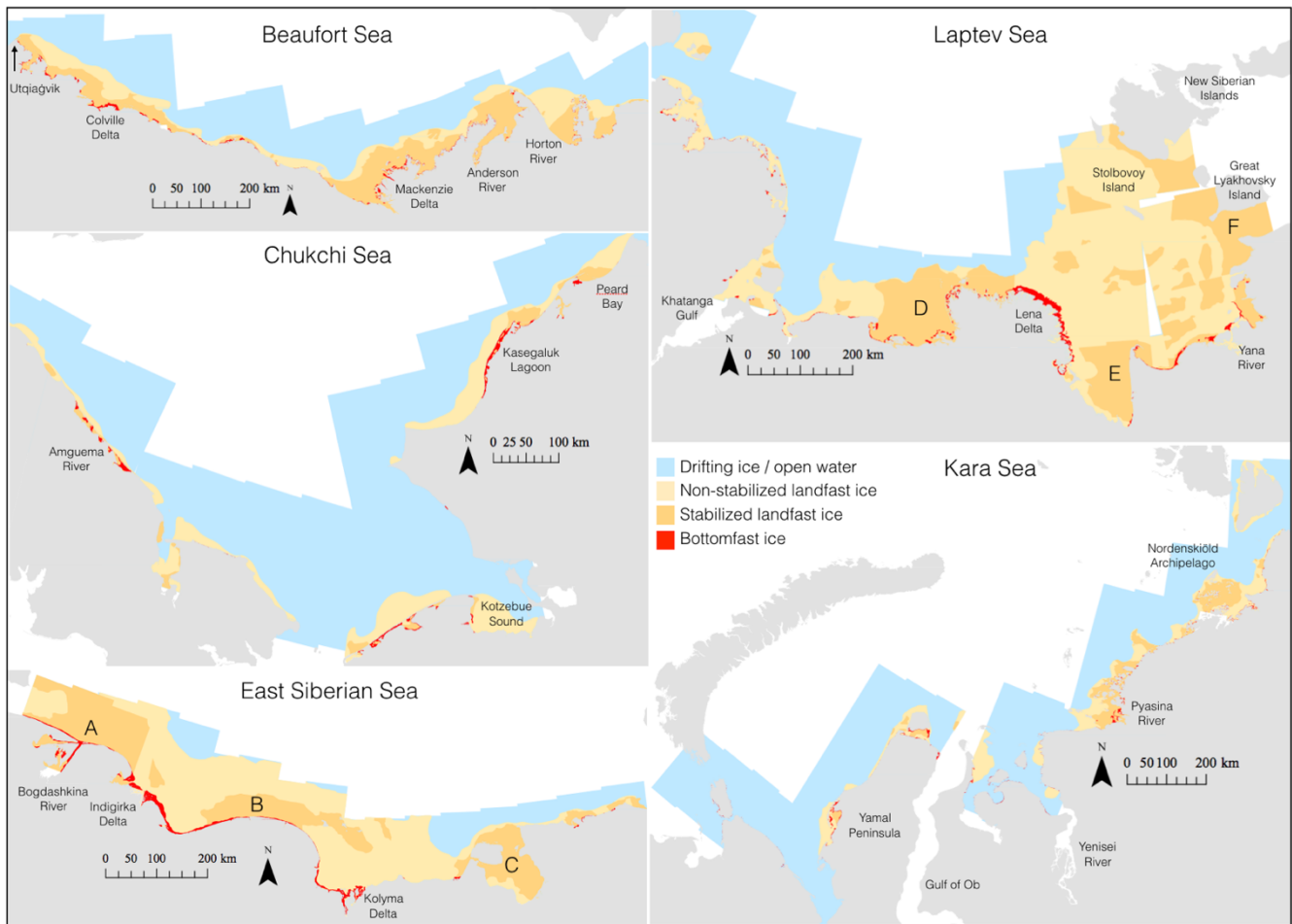
Figure 9: InSAR-derived map of non-stabilized and stabilized landfast ice and bottomfast ice from Sentinel-1 image pairs, acquired predominantly between March and May, 2017. Letters "A" - "G" mark areas discussed in the text. Land is masked out in light grey. This map of stability zones is subject to limitations and uncertainties outlined in the text.
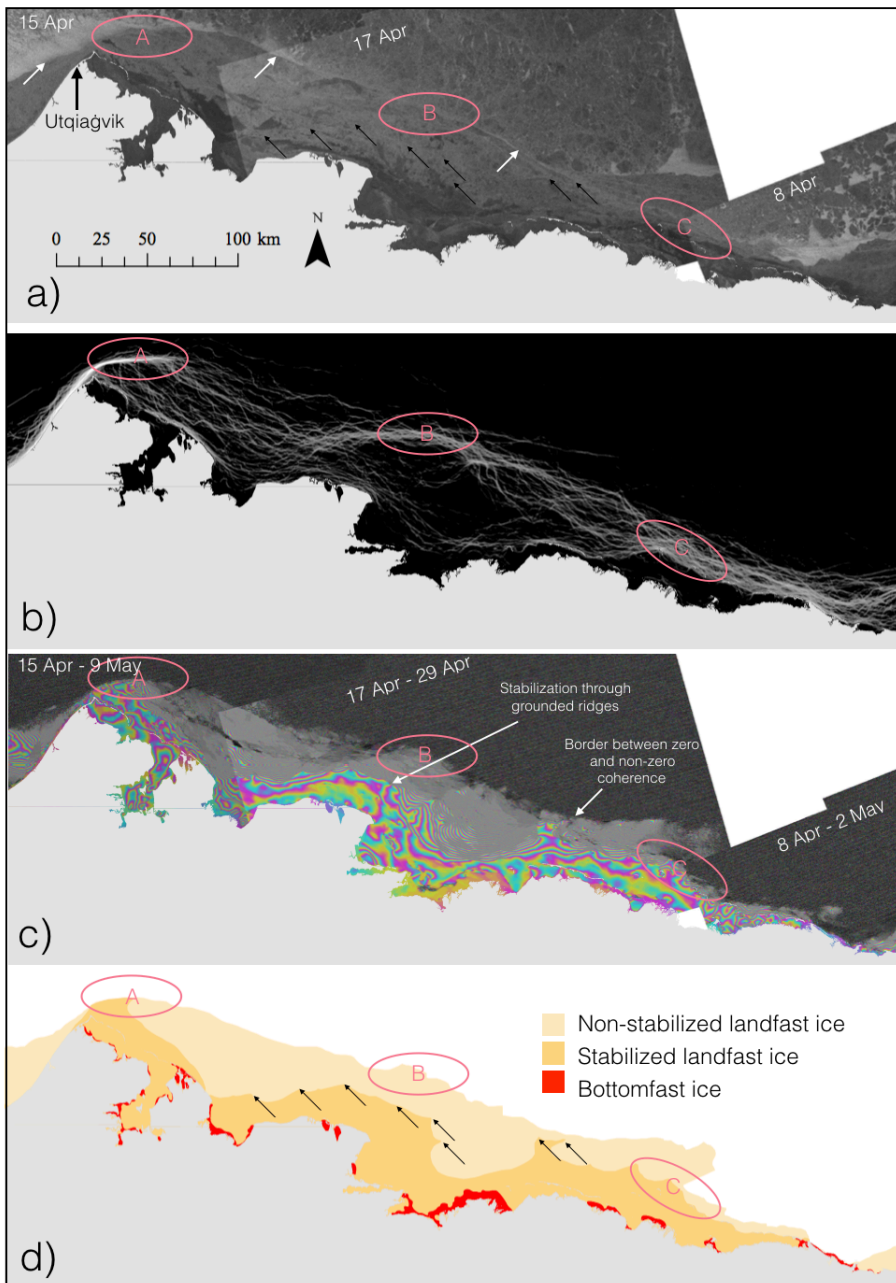
Figure 10: (a) Sentinel-1 backscatter images over the western Beaufort Sea. White arrows signify the landfast ice edge as identified by contrasting backscatter. (b) Landfast ice edge occurrence mapped for the period 1996–2008 over the Alaska Beaufort Sea (Mahoney et al. 2014). Light red circles correspond to areas of frequent landfast ice edge formation, referred to as "nodes. (c) Interferograms between mid-April and mid-May 2017. (d) Different stability zones derived from (c). Potential grounding points as identified in (d) are marked with black arrows in (d) and (a). Land is masked out in light gray.
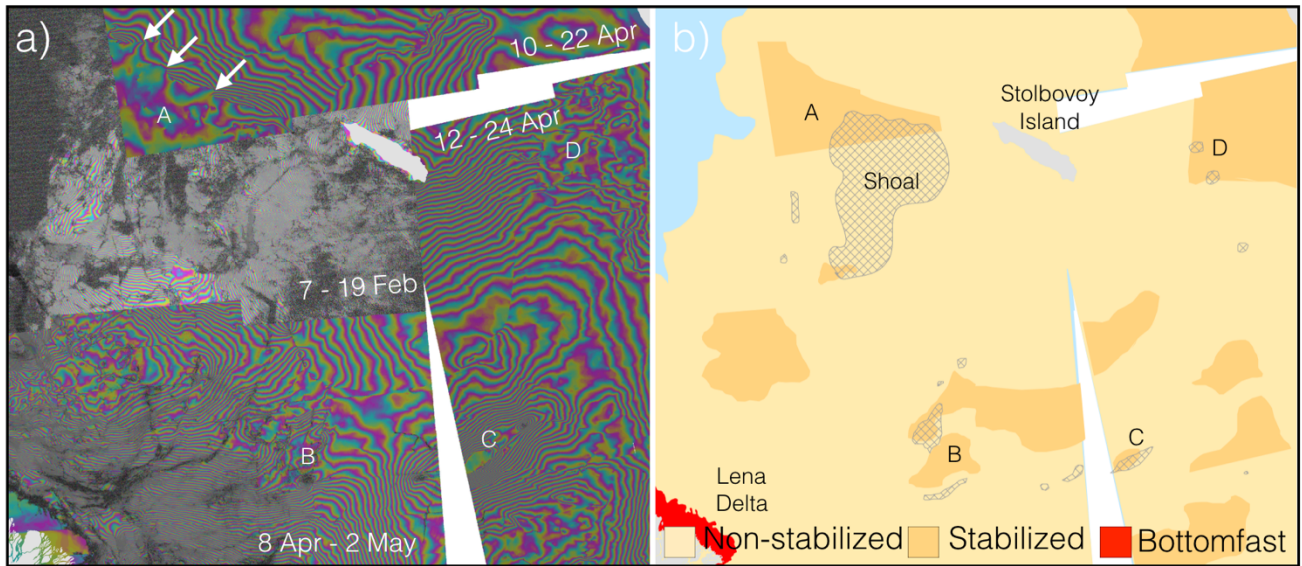
Figure 11: (a) Sentinel-1 interferograms over Laptev Sea near Stolbovoy Island between February and May 2017. (b) Outlined non-stabilized (light orange) and stabilized (dark orange) ice. Shallow areas (<10 m; Jakobsson et al., 2012) are marked with gray cross hatching. Stabilized ice that is likely supported by grounding near shallow features are marked "A"-"D" and further discussed in the text. Land is masked out in light gray.
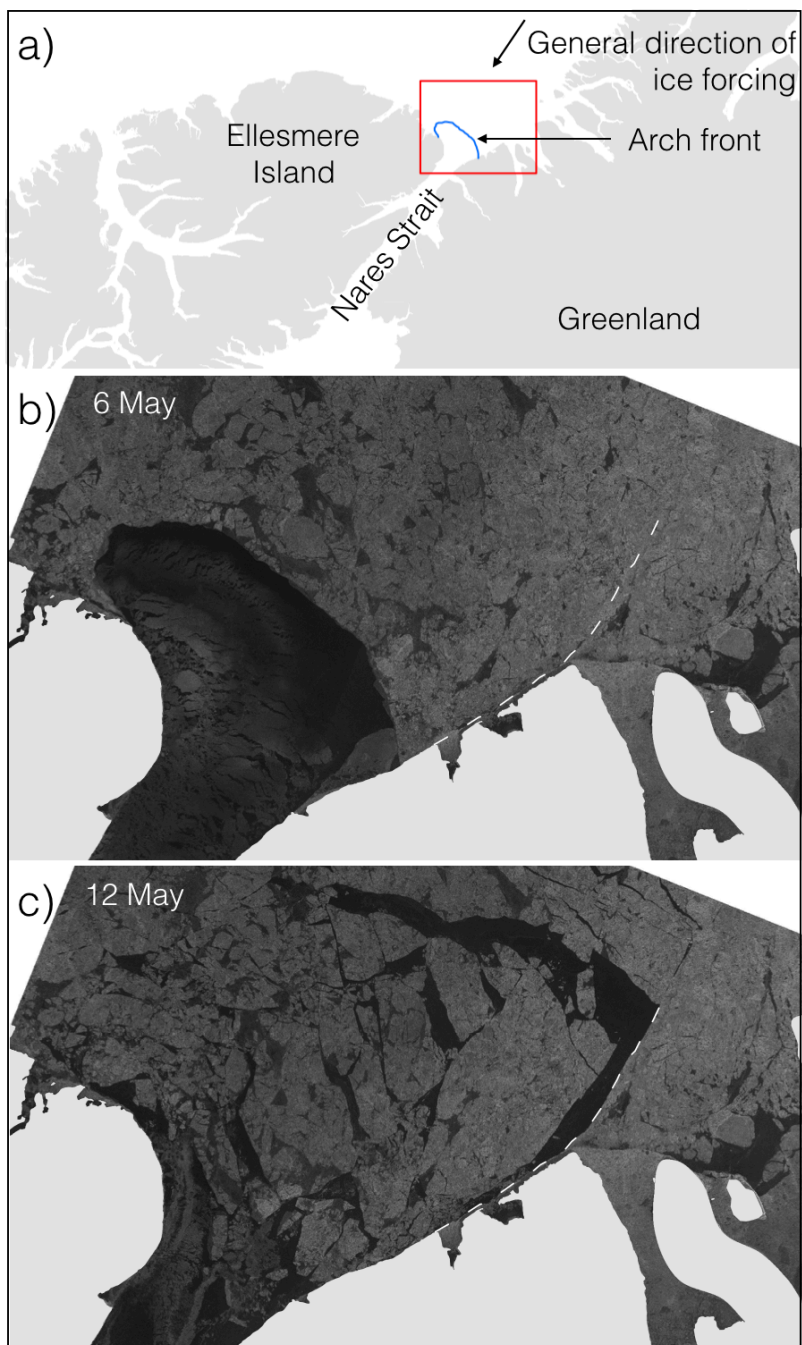
Figure 12: Map of Nares Strait (a), and Sentinel-1 backscatter images over the 2017 ice arch (blue line in a) before (b) and after (c) failure. The line of failure is identified in (c) and marked as a dashed line in both (b) and (c). Land is masked out in light gray.
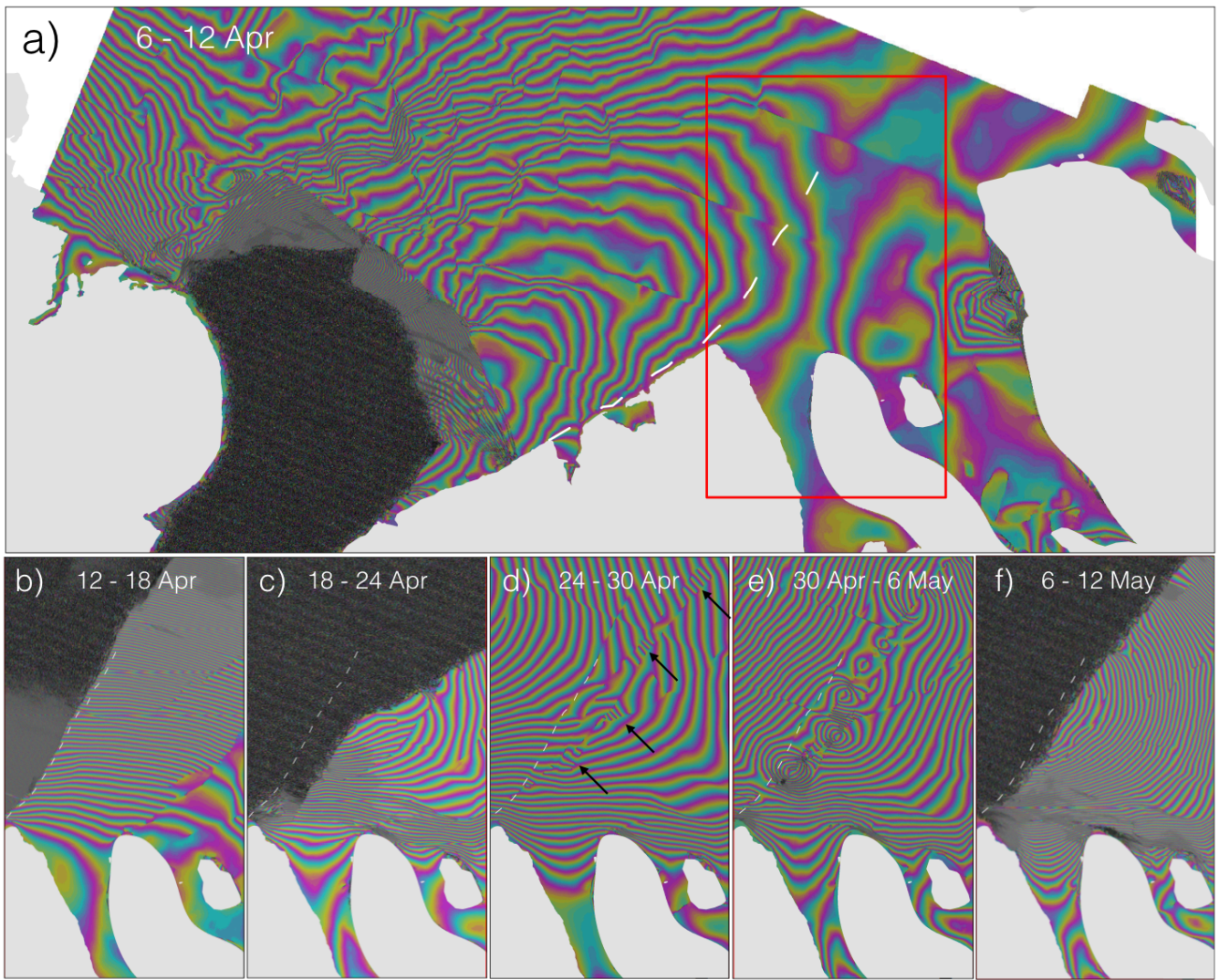
Figure 13: Interferogram over the Nares Strait ice arch in 2017, covering the time period 6-12 Apr (a). Smaller panels show consecutive interferograms within the box for 12 - 18 Apr (b); 18 - 24 Apr (c); 24 - 30 Apr (d); 30 Apr - 6 May (e); and 6 - 12 May (f). Dashed line represents the line separating fast and moving ice in Figure 12c. The black arrows in (d) indicate fringe patterns further discussed in the text. Land is masked out in light gray.

Table 1: Landfast sea ice stability regimes and assigned stability zones identified using InSAR

	Landfast ice regime	Stability	Stability zone	Identified by
1	Bottomfast sea ice (i.e., ice frozen to or in broad contact with the sea floor)	Completely stable. Ice is frozen to or resting on the sea floor, restricting lateral motion. Vertical tide jacking may occur as the ice thickens.	Bottomfast	No identifiable phase difference from the adjacent land
2	Floating ice sheltered by point features, such as grounded ridges or islands, or fully enclosed in lagoons or fjords	Moderate stability. Ice is supported by coastlines or point features, completely or largely inhibiting break out events. In addition to thermal creep, internal stress from more dynamic ice can propagate in between pinning points, resulting in dm- to m-scale non-elastic deformation.	Stabilized	Poorly defined, widely spaced fringes, or abruptly reduced fringe spacing compared to offshore ice
3	Floating ice extensions	Low stability. Dominated by m-scale deformation from ice, wind, and ocean forcing. Persistent inelastic deformation can lead to accumulated strain on the order of tens of meters on time-scales exceeding several weeks. Ice may remain attached (Mahoney et al., 2004) or can break-off from the stabilized ice.	Non-stabilized	Well-defined fringe orientation or patterns

Table 2: Approximate area coverage of landfast ice (in thousand km^2).

Area	Bottomfast	Stabilized	Non-stabilized	Total area of landfast ice	Area fraction: non-stabilized / stabilized
Beaufort Sea	2.5	35	29	67	0.83
Chukchi Sea	1.8	4.6	25	31	5.43
East Siberian Sea	5.1	45	80	130	1.78
Laptev Sea	4.1	74	127	205	1.72
Kara Sea	2.6	16	37	56	2.3

The bottomfast ice zone is constrained between its outer extent (interpreted from the phase) and the coast (as interpreted from the backscatter scenes). The stabilized zone is constrained between its outer extent (as interpreted from the phase) and the bottomfast ice or the landmask (Wessel and Smith, 1996). The non-stabilized ice is constrained between the outer extent of non-zero coherence and the bottomfast ice, stabilized ice, or the landmask.